The Canadian Mineralogist
Vol. 32, pp. 781-801 (1994)

METAMORPHISM OF PELITIC ROCKS IN THE PALEOPROTEROZOIC RAMAH GROUP, SAGLEK AREA, NORTHERN LABRADOR: MINERAL REACTIONS, P–T CONDITIONS AND INFLUENCE OF BULK COMPOSITION

FLEMMING MENGEL

Geological Museum, Østervoldgade 5–7, 1350 Copenhagen K, Denmark

TOBY RIVERS

Department of Earth Sciences, Memorial University of Newfoundland, St. John's, Newfoundland A1B 3X5

ABSTRACT

Mineral assemblages in metapelitic rocks of the Ramah Group from the externides of the Torngat Orogen near Saglek Fiord, northern Labrador have been analyzed in detail. A progression from the upper greenschist to the middle amphibolite facies is preserved along the metamorphic field-gradient, and six metamorphic zones have been defined based on the following mineral assemblages: Zone 1: Chl–Bt; Zone 2: Cld–Chl–And; Zone 3: Cld–Chl–Ky; Zone 4: St–Chl; Zone 5: Ky–Bt; and Zone 6: Sil–St–Bt, Grt–Bt, and Grt–St–Bt. Reaction isograds separating the zones are as follows: And = Ky between zones 2 and 3, Cld + Ky = St + Chl between zones 3 and 4, St + Chl = Ky + Bt between zones 4 and 5, and Ky = Sil between zones 5 and 6. Qualitative and quantitative P–T estimates suggest variation along the metamorphic field-gradient from ≤ 3 kbar and 450°C to ≤ 7 kbar and 650°C. The pelites have low concentrations of minor (*i.e.*, non-KFMASH) components and intermediate X_{Mg}, resulting in the stability of chlorite up to middle-amphibolite-facies conditions and restriction of garnet to the highest-grade assemblages. Variations in both bulk-rock Al content and tie-line topologies controlled Al-saturation in the mineral assemblages. At low grades, only the Al-rich bulk compositions were Al-saturated, with reactions involving the Tschermak exchange vector affecting the position of the Al-saturation surface. At higher grades, after the Cld–Chl and St–Chl tie-lines became unstable, Al-saturation was possible in Al-poorer rocks containing biotite. There are systematic variations in X_{Mg} distribution between coexisting Ms, Bt, Chl and possibly Cld that do not seem attributable to the presence of ferric iron in these minerals. This is consistent with the presence of non-ideal mixing in the Ms–Cd and possibly Chl solid solutions.

Keywords: muscovite, kyanite, andalusite, sillimanite, biotite, chloritoid, staurolite, chlorite, Torngat Orogen, Ramah Group, Saglek, Labrador.

SOMMAIRE

Les assemblages de minéraux des roches métapélitiques du Groupe de Ramah, du secteur externe de l'orogène de Torngat, près du fjord de Saglek, dans le nord du Labrador ont été étudiés en détail. Une progression à partir du faciès schistes verts supérieur au faciès amphibolite moyen est préservée le long d'un gradient métamorphique sur le terrain. Six zones métamorphiques ont été définies selon les assemblages suivants: Chl–Bt (zone 1), Cld–Chl–And (zone 2), Cld–Chl–Ky (zone 3), St–Chl (zone 4), Ky–Bt (zone 5), et Sil–St–Bt, Grt–Bt et Grt–St–Bt (zone 6). Les réactions isogrades suivantes séparent les zones: And = Ky entre les zones 2 et 3, Cld + Ky = St + Chl entre les zones 3 et 4, St + Chl = Ky + Bt entre les zones 4 et 5, et Ky = Sil entre les zones 5 et 6. Un estimé qualitatif et quantitatif de la pression et de la température indique un gradient de ≤3 kbar et 450°C jusqu'à ≤7 kbar et 650°C. Les pélites possèdent une faible teneur en composants mineurs (c'est-à-dire, ne faisant pas partie du système KFMASH), et une valeur intermédiaire de X_{Mg}, ce qui rend compte de la stabilité de la chlorite jusqu'au faciès amphibolite moyen, et de la restriction du grenat aux assemblages des niveaux métamorphiques les plus élevés. Les teneurs en Al des roches et la topologie des lignes de coexistence ont régi les assemblages de minéraux. Dans les zones de métamorphisme de faible intensité, seules les compositions fortement alumineuses étaient saturées en Al; les réactions impliquant le vecteur d'échange Tschermak ont influencé la position de la surface de saturation en Al. Aux niveaux plus élevés, une fois les lignes de coexistence Cld–Chl et St–Chl rompues, la saturation en Al est devenue possible dans les roches à plus faible teneur en Al, contenant la biotite. Nous décelons des variations systématiques dans la distribution de X_{Mg} parmi Ms, Bt, Chl et peut-être même Cld coexistants qui ne semblent pas attribuables à la présence du Fe^{3+} dans ces minéraux. Ceci concorde avec la possibilité de mélange non-idéal dans les solutions solides Ms–Cd et peut-être Chl.

(Traduit par la Rédaction)

Mots-clés: muscovite, kyanite, andalousite, sillimanite, biotite, chloritoïde, staurotide, chlorite, orogenèse de Torngat, Groupe de Ramah, Saglek, Labrador.

INTRODUCTION

Petrographic observations of reaction relationships and of the relative chronology of mineral growth, if combined with the chemical compositions of coexisting minerals, can provide important information about the metamorphic evolution at specific locations along a metamorphic field-gradient. In favorable circumstances, the sequence of metamorphic reactions can be determined from the compositional evolution of coexisting minerals, and the role of variations in bulk composition in controlling the mineral assemblages can be assessed. Through qualitative or quantitative thermobarometry, the P–T–*X* conditions under which these reactions took place may then be estimated or approximated.

This communication comprises a detailed description and interpretation of reaction microstructures, assemblages of stable minerals and estimated P–T conditions of pelites along a metamorphic field-gradient through the Paleoproterozoic Ramah Group in the vicinity of Saglek Fiord, northern Labrador (Fig. 1). This area lies near the eastern margin of Torngat Orogen (Hoffman 1988, Mengel 1988) and was deformed and metamorphosed about 1850–1800 Ma ago.

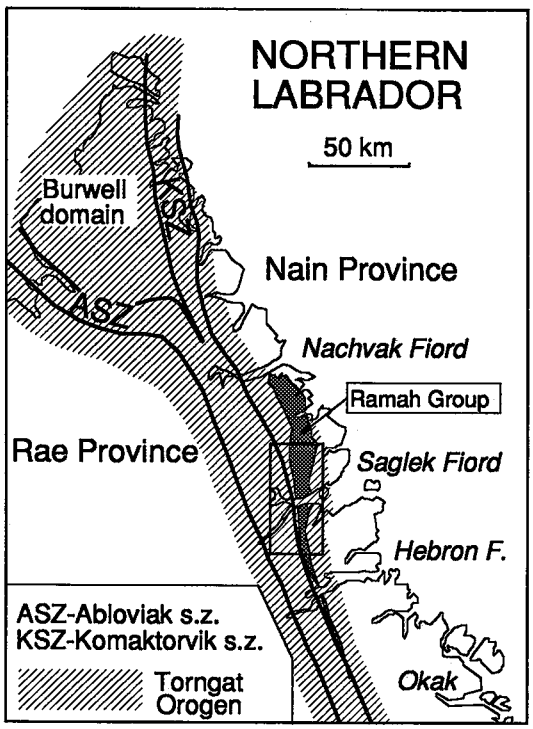

FIG. 1. Simplified lithotectonic map of northern Labrador showing the tectonic subdivisions and the location of the Ramah Group. The box shows the location of Fig. 4 (s.z.: shear zone).

REGIONAL SETTING

The Ramah Group was deposited unconformably on stabilized Archean crust after intrusion of a regional swarm of basic dykes, but before any Proterozoic thermotectonic effects. Its present area of outcrop straddles the boundary between the Archean Nain Province to the east and the transcurrent Abloviak shear zone in the core of Torngat Orogen to the west. Deformation and metamorphism in the Ramah Group are thus representative of the Torngat Front (*i.e.*, the eastern limit of deformation associated with the Torngat Orogen: Mengel *et al.* 1991).

The Torngat Orogen contains evidence of several phases and styles of deformation interpreted to have formed in a zone of oblique continental collision between the Archean Nain and Rae provinces (Mengel 1988, Hoffman 1988, Ermanovics *et al.* 1989, Van Kranendonk 1990, 1992, Van Kranendonk & Ermanovics 1990, Mengel *et al.* 1991). In the eastern part of the orogen, early east-directed crustal thickening in a thrust regime was followed by penetrative, sinistral transcurrent shearing in the Abloviak shear zone, which in turn was followed by a second stage of east-directed thrusting and reverse faulting that resulted in telescoping of the metamorphic field-gradient across strike and exhumation of the high-grade internides over the lower-grade externides of the orogen.

THE RAMAH GROUP

In the northwestern part of its outcrop, the Ramah Group is preserved in a foreland fold–thrust belt (Mengel *et al.* 1991, Calon & Jamison 1993), whereas farther south it was involved in the Abloviak shear zone (Ermanovics *et al.* 1989, Ermanovics & Van Kranendonk 1990, Van Kranendonk 1990, 1992). There is significant regional north–south variation in the level of exposure, and hence in structures and metamorphism, in the Ramah Group throughout its area of outcrop. In Nachvak Fiord (Fig. 1), the base of the Ramah Group is exposed in cliffs well above sea level, and Wardle (1983) has noted the presence of a basal thrust in basement gneisses beneath the Ramah Group. At Saglek Fiord, the Ramah Group is exposed at sea level, and the basal thrust is only exposed to the east of the outcrop of the Ramah Group (Mengel 1988; Fig. 2). Between Hebron and Okak Fiord (Fig. 1), the outcrop width of the Ramah Group decreases substantially, and the unit occurs as highly deformed discontinuous slivers in the eastern part of the Abloviak shear zone.

The intensity of deformation and metamorphism also increases from east to west, perpendicular to the strike of the Torngat Orogen. Immediately south of Nachvak Fiord (Fig. 1), the eastern exposures of the Ramah Group lie to the east of the Torngat Front, and

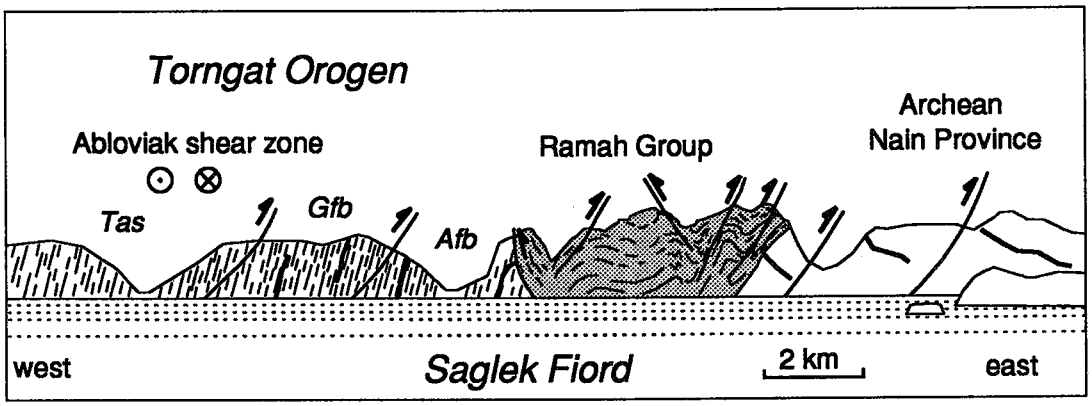

FIG. 2. Schematic section along the north shore of Saglek Fiord showing the distribution of lithological units and major structures. The steep mylonitic fabric in the Abloviak shear zone is truncated by east-directed, west-dipping thrusts. Thick lines represent Proterozoic dykes. Abbreviations: Tas: Tasiuyak gneiss, Gfb: granulite-facies block, Afb: amphibolite-facies block.

were little affected by Torngat Orogeny. West of the Torngat Front in the fold–thrust belt, the grade of metamorphism in the Ramah Group increases toward the west in the structurally higher thrust-slices. There is also an increase in structural complexity and metamorphic grade southward, accompanying the narrowing of the outcrop of the Ramah Group. The western margin of the Ramah Group is limited by steep thrust-faults throughout its length.

The Ramah Group is predominantly of sedimentary origin. This paper is concerned with metamorphism of rocks of the Rowsell Harbour, Reddick Bight and Nullataktok formations, which consist of sandstone, mudstone, greywacke and black shale and their metamorphic equivalents (Knight 1973, Morgan 1975, Knight & Morgan 1977, 1981).

Penetrative structures in the Ramah Group at the latitude of Saglek Fiord are interpreted to be of three generations. D_1 and D_2, which account for the main structures in the fold–thrust belt, appear to be kinematically related and may not be much separated in time. Bedding (S_0) is commonly preserved, and S_1 is defined as a slaty cleavage or schistosity (see, for example, Fig. 3a). S_1 is generally parallel to S_0, but in thin section it can commonly be seen that the two are separated by a small angle, indicating the widespread occurrence of associated isoclinal F_1 folds. However, F_1 fold hinges are observed only locally as intrafolial rootless folds of quartzite layers in slate. The D_1 structures are interpreted to have formed in a thrusting event that resulted in east-directed tectonic transport and thickening of the Ramah Group over the Nain craton (Mengel *et al.* 1991, Calon & Jamison 1993).

S_2 is a variably developed, steeply west-dipping crenulation cleavage (*e.g.*, Fig. 3a). North of Saglek Fiord, the intensity of S_2 varies from weak in the east to moderate in the west. Farther south, especially southwest of Pangertok Inlet (Fig. 4), transposition of S_1 into S_2 is widespread, and S_2 becomes the main foliation (*e.g.*, Figs. 3c–f). Throughout much of the study area, open to tight F_2 folds with north-trending, subhorizontal to gently plunging axes and vertical to steeply west-dipping axial surfaces (S_2) dominate the map pattern. Microstructural relationships indicate that the highest-grade metamorphic assemblages formed syn-D_2 [and also late-D_1 in the Lake Kiki region according to Calon & Jamison (1993)].

Weakly developed F_3 folds occur locally south of Saglek Fiord. These deform S_2 into open asymmetrical southwest-verging cross-folds with northwest-trending subhorizontal axes. An axial-planar cleavage is not developed.

In the study area, metamorphic grade in the Ramah Group varies from greenschist to lower amphibolite facies. In the eastern half of the Ramah Group, chloritoid is present in Al-rich units north and immediately south of Saglek Fiord, whereas higher metamorphic grades farther west are recorded by andalusite-, staurolite- and kyanite-bearing assemblages in mica schists. Farther south, increasing grade is recorded by garnet-, staurolite- and sillimanite-bearing assemblages in rocks of suitable composition.

The metamorphic zonation in the Torngat Orogen, including that of the Ramah Group, is telescoped by east-directed movement on west-dipping thrusts and reverse faults, which has accentuated the range in metamorphic parageneses across the outcrop width of the Ramah Group (further described below). A more gradual southerly increase in metamorphic grade, coincident with the narrowing of the outcrop width of Ramah Group in that direction, also is apparent.

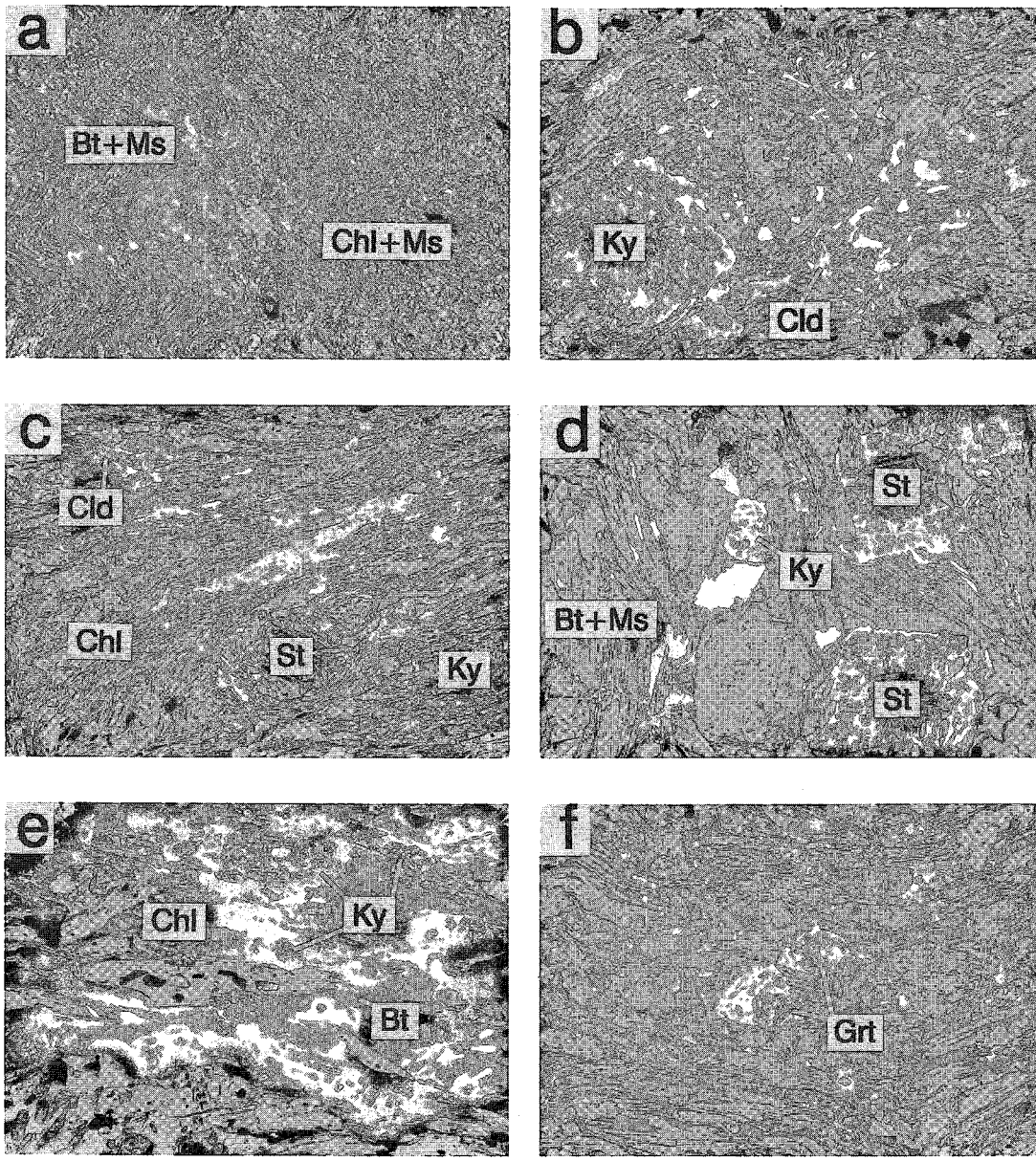

FIG. 3. Photomicrographs showing various microstructural and paragenetic features in the Ramah Group metapelites. Longest dimension of photos: 4.5 mm (a), 1 mm (b, c, e), 2.1 mm (d, f). (a): Compositional layering (S_0) in mica schist. Bt–Ms predominate mineralogy in left side of image, whereas Chl–Ms predominate in right side. S_1 is broadly parallel to S_0, and both are affected by D_2 crenulation (S_1 and S_0 vertical, S_2 horizontal). Sample F84–28, ppl (plane-polarized light). (b): The Zone-3 assemblage Ky–Cld–Ms–Qtz. Muscovite and quartz are present throughout the matrix. The dominant fabric is S_2. Sample F83–62, ppl. (c): The assemblage Cld–Ky–St–Chl–Ms–Qtz, marking the reaction isograd separating Zones 3 and 4. Muscovite and quartz present throughout the matrix. The dominant fabric is S_2. Sample F84–377, ppl. (d): The assemblage St–Chl–Ky–Bt–Ms–Qtz, marking the reaction isograd separating Zones 4 and 5. Muscovite, chlorite and quartz present throughout the matrix. Sample F83–79, ppl. (e): The Zone-5 assemblage Ky–Bt–Chl–Ms–Qtz. The dominant fabric is S_2. Muscovite and quartz present throughout the matrix. Sample F83–76, ppl. (f): The "Zone 6" assemblage Grt–Bt–Ms–Qtz. The dominant fabric is S_2. Biotite, muscovite (note intergrowths) and quartz present throughout the matrix. Sample F83–131, ppl.

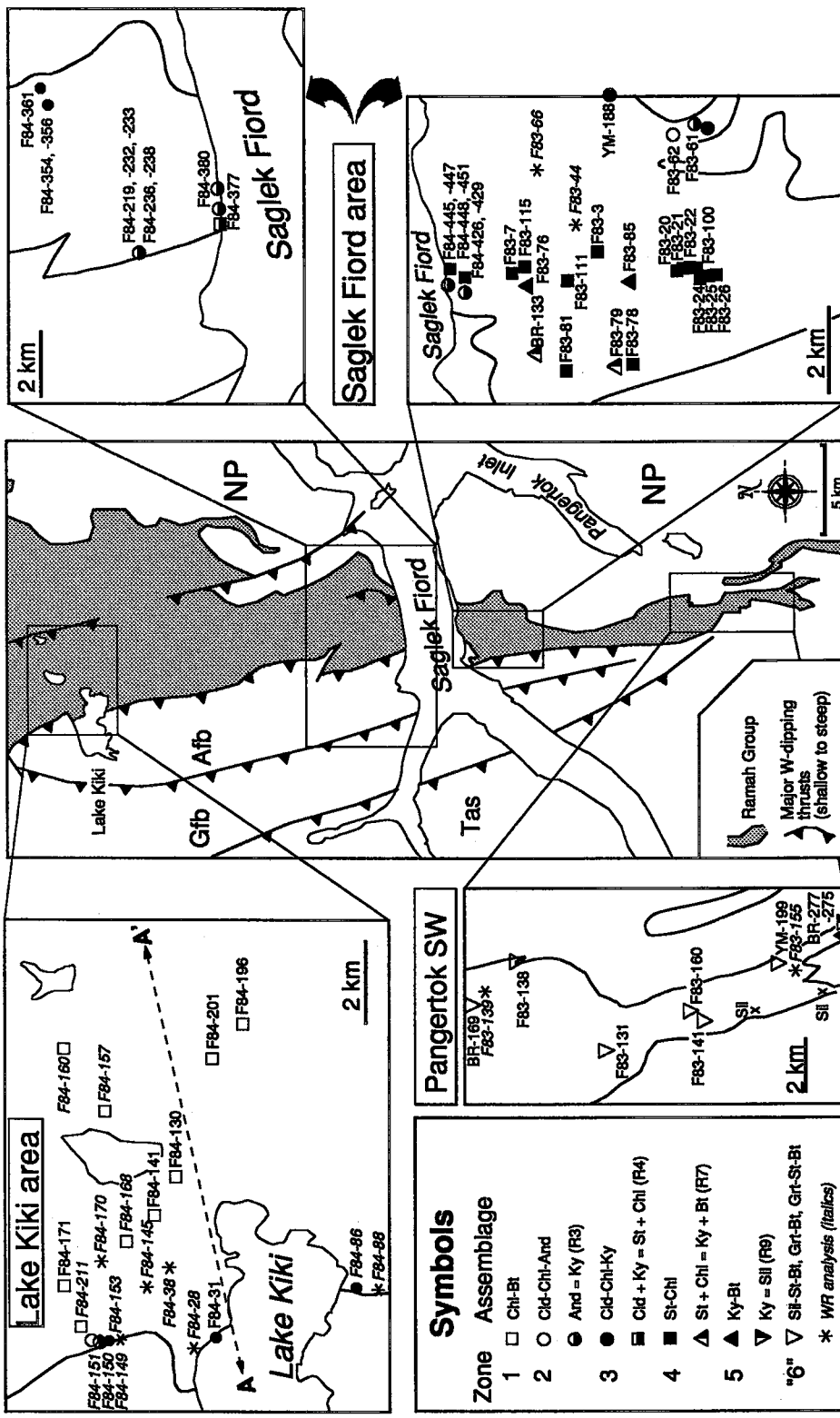

FIG. 4. Schematic map of the Ramah Group and adjacent lithotectonic units in the Saglek Fiord region, showing the location of the samples investigated (see also Tables 1–3) and the regional distribution of metamorphic zones and assemblages. For clarity, the boundaries between metamorphic zones have not been drawn. The location of the Lake Kiki transect (Fig. 4) is also indicated (A–A'). Abbreviations: Tas: Tasiuyak gneiss, Gfb: granulite-facies block, Afb: amphibolite-facies block, NP: Nain Province, WR: whole rock. Mineral abbreviations from Kretz (1983).

Bulk Chemistry of the Pelites

It is useful to consider the variations in bulk composition among pelitic rocks of the Ramah Group as a prelude to the discussion and interpretation of paragenetic and mineral chemical data. To this end, bulk-chemical analyses of twenty samples of pelitic schists were performed (Table 1). The analyzed rocks come from east of Lake Kiki (n = 14), immediately north and south of Saglek Fiord (n = 3), and southwest of Pangertok Inlet (n = 3). In the remainder of this text, these three areas will be referred to as the Lake Kiki, Saglek Fiord and Pangertok SW areas, respectively. Figure 4 shows the location of analyzed samples, and the Appendix contains analytical details.

The Lake Kiki area was considered especially amenable to such a study because the Rowsell Harbour, Reddick Bight, and Nullataktok formations are all represented in the cross-section. Owing to advanced recrystallization and structural complexity, the few samples from the two other areas have not been assigned to any particular formation, except for F83–44 and –124 in the Saglek Fiord area, which were collected from recognizable exposures of the Nullataktok Formation.

Figure 5 shows that in the western part of the Lake Kiki section, there is substantial chemical variation among samples of the Rowsell Harbour and Reddick Bight formations (most oxides). In the eastern part of the section, the Nullataktok Formation displays somewhat greater homogeneity (apart from a rather erratic westward increase in SiO_2). With the exception of a single sample, F83–66, which is higher in Mg and lower in Al, samples from the Saglek Fiord and Pangertok SW areas are similar to those from the Lake Kiki section and are not plotted. F83–66 is the only sample from the upper part of the Nullataktok Formation, which may account for its different chemistry.

Variations in MgO, FeO, K_2O and Al_2O_3 are especially important in metapelites, and these can conveniently be illustrated in the AFM diagram (Thompson 1957). The data are plotted in Figure 6. Since Fe^{3+} (and hence Fe^{2+}/Fe^{3+}) was not determined on rocks from the Saglek Fiord and Pangertok SW sections, the following observations apply only to samples from the Lake Kiki section. Compositionally, the rocks range from "Al-rich" to "Fe-rich" pelites (nomenclature of Powell 1978, p. 217). The distribution clearly reflects the differences between the Reddick Bight and Rowsell Harbour formations and the Nullataktok Formation. Similar differences are shown by the oxidation ratio (Table 1, Fig. 5). Reddick Bight and Rowsell Harbour formations show a wide range of oxidation ratio ($24 < OR < 85$), in contrast to a more restricted, lower range in the Nullataktok Formation ($10 < OR < 47$).

The AKF diagram also serves to distinguish the composition of the Nullataktok Formation from those of the Reddick Bight and Rowsell Harbour formations (Fig. 6). Samples of the Reddick Bight and Rowsell Harbour formations display a larger range in A/F ratio than those from the Nullataktok Formation. The wide range of compositions has resulted in an exceptional range of mineral assemblages in the Ramah Group, as is discussed below.

TABLE 1. MAJOR-ELEMENT CHEMISTRY OF SELECTED RAMAH GROUP METAPELITES

Sample:	F84-86	F84-28	F84-88	F84-149	F84-150	F84-151	F84-153	F84-211	F84-145	F84-38	F84-170	F84-168	F84-157	F84-160	F83-44	F83-66	F83-124	F83-139	F83-155	F83-160
Area:	Kiki E	Kiki E	Kiki E	Kiki E	Kiki E	Kiki E	Kiki E	Kiki E	Kiki E	Kiki E	Kiki E	Kiki E	Kiki E	Kiki E	Sagl F	Sagl F	Sagl F	Pan SW	Pan SW	Pan SW
Lith.:	RBRH	RBRH	RBRH	RBRH	RBRH	RBRH	RBRH	RBRH	NULL	NULL	NULL	NULL	NULL	NULL	NULL	?	NULL	?	?	?
SiO2 wt%	58.10	51.80	77.30	50.40	58.20	59.40	62.00	59.10	58.10	68.80	57.20	62.70	52.10	53.80	63.00	58.20	63.50	67.90	65.20	63.30
TiO2	0.32	1.04	0.16	0.96	0.72	0.92	0.24	1.20	0.80	0.56	0.88	0.96	2.12	1.76	0.80	1.04	0.84	0.68	0.56	0.84
Al2O3	21.40	18.90	9.82	22.60	20.20	13.30	16.00	17.10	14.30	15.40	11.10	13.30	18.80	18.60	18.40	11.20	17.90	16.30	18.30	18.50
FeO	4.35	9.17	2.30	1.76	4.07	2.55	3.79	6.93	9.31	1.47	8.28	8.11	11.83	10.90						
Fe2O3	2.59	4.23	2.38	11.06	4.37	15.31	6.63	2.89	1.26	1.46	0.95	1.24	1.91	2.39	5.43*	12.85*	6.17*	4.59*	3.79*	6.06*
MnO	0.03	0.09	0.03	0.02	0.04	0.01	0.04	0.02	0.08	0.04	0.09	0.04	0.07	0.05	0.08	0.11	0.07	0.02	0.03	0.05
MgO	2.88	4.44	1.60	1.27	2.02	1.09	2.54	2.68	4.45	2.70	4.89	4.28	2.44	2.08	1.92	9.99	2.13	1.71	1.90	1.91
CaO	0.10	2.00	0.52	0.54	0.28	0.26	0.26	0.14	2.16	0.24	5.66	1.00	0.38	0.24	0.18	0.40	0.16	0.28	1.04	0.12
Na2O	0.69	0.72	0.35	1.43	0.70	0.66	0.41	2.05	1.72	1.49	0.62	1.76	1.06	1.33	1.01	0.06	1.07	1.08	1.72	0.50
K2O	4.47	1.57	1.94	4.25	4.27	2.85	3.55	3.14	4.39	3.60	2.76	2.98	4.91	3.85	6.07	2.31	6.05	5.70	5.01	6.05
P2O5	0.05	0.04	0.02	0.33	0.12	0.17	0.12	0.00	0.00	0.00	0.03	0.02	0.03	0.05	0.00	0.14	0.02	0.00	0.00	0.05
LOI	4.38	4.99	2.25	4.17	3.88	2.41	3.39	5.23	2.10	4.33	8.19	4.09	4.32	4.62	2.22	3.92	2.56	1.90	1.97	2.39
SUM	99.36	98.99	98.67	98.79	98.87	98.93	98.97	100.48	98.67	100.09	100.65	100.48	99.97	99.67	99.11	100.22	100.47	100.16	99.52	99.77
FeOT**	6.68	12.98	4.44	11.71	8.00	16.33	9.76	9.53	10.44	2.78	9.14	9.23	13.55	13.05						
Fe2O3T**	7.42	14.41	4.93	13.01	8.89	18.14	10.84	10.58	11.59	3.09	10.14	10.24	15.04	14.49						
OR	35	24	48	85	49	84	61	27	11	47	9	12	13	17						

*) Total iron expressed as Fe2O3; **) FeOT = FeO + 0.9Fe2O3 and Fe2O3T = Fe2O3 + 1.1FeO

Areas: Kiki E - transect east of Lake Kiki, Sagl F - Saglek Fiord, Pan SW - Pangertok SW (areas defined in text)

Lithologies: RBRH - Reddick Bight or Rowsell Harbour formations, NULL - Nullataktok Formation, ? - formation not known with certainty

OR - oxidation ratio, calculated as (2[Fe2O3]/2[Fe2O3]+[FeO])*100 (Chinner, 1960), where [] indicates molar proportions of oxides.

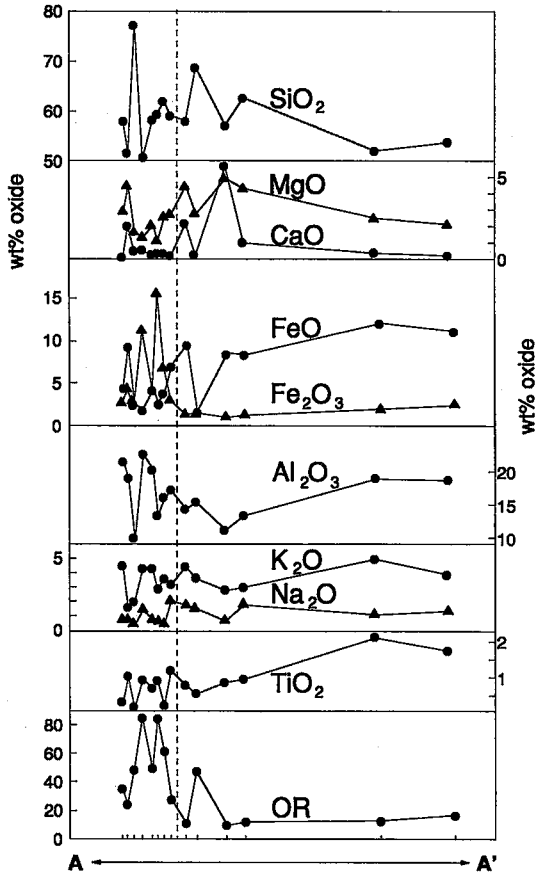

FIG. 5. Bulk-chemical variations in Ramah Group pelites east of Lake Kiki. Concentrations of selected major elements are projected onto an ENE–WSW section (for location, see Fig. 4). Small tics along A–A′ represent locations of samples. The dashed line separates Nullataktok Formation (east) from Rowsell Harbour and Reddick Bight formations (west). OR: oxidation ratio (see Table 1).

MINERAL ASSEMBLAGES

Pelitic rocks of the Ramah Group have been examined in three traverses (near Lake Kiki, along Saglek Fiord, and southwest of Pangertok Inlet). The locations of traverses and of all samples utilized in this study are shown in Figure 4. The mineral assemblages in pelitic rocks in the Ramah Group have been subdivided into six metamorphic zones separated by four reaction isograds on the basis of diagnostic mineral assemblages. Representative mineral compositions are given in Tables 2 and 3. Values of X_{Mg} [= Mg/(Mg+Fe), where Fe is total iron calculated as Fe^{2+}] of coexisting minerals, are given in Figure 7.

All assemblages contain muscovite and quartz in addition to the phases discussed, and an aqueous vapor phase with unit activity is presumed to have been present during metamorphism, unless otherwise noted. The terms "divariant" and "univariant" are used with reference to the "ideal" KFMASH system of Thompson (1957). Mineral abbreviations are after Kretz (1983).

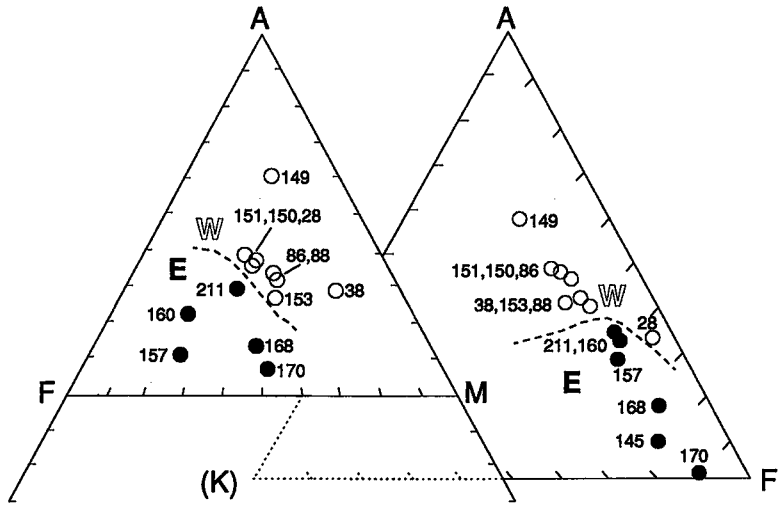

FIG. 6. Compositions of selected samples of Ramah Group pelites from the Lake Kiki transect plotted in AFM and AKF diagrams. Open symbols represent samples from the Rowsell Harbour and Reddick Bight formations (W: western part of section in Fig. 3), and filled symbols correspond to Nullataktok Formation pelites (E: eastern part). All sample numbers have prefix "F84–".

TABLE 2. REPRESENTATIVE COMPOSITIONS OF MINERALS FROM ZONES 1-4 IN RAMAH GROUP METAPELITES

Sample	F84-211	F84-211	F84-211	F83-61	F83-61	F84-377	F84-377	F84-377	F84-377	F83-3	F83-3	F83-3	F83-22	F83-22	F83-22	F83-22
Zone	1	1	1	2/3	2/3	3/4	3/4	3/4	3/4	4	4	4	4	4	4	4
Mineral	Bt	Chl	Ms	Cld	Ms	St	Chl	Cld	Ms	Ms	St	Chl	Ms	Bt	Chl	St
Code	P2	P11	P16	P2	P6	P1	P2	P6	P8	P2	P3	P5	P1	P3	P6	P13
SiO2 wt%	35.38	24.33	46.86	25.11	45.48	27.98	25.48	25.15	45.10	45.76	28.04	26.65	48.39	37.24	23.93	28.70
TiO2	1.60	0.09	0.41	0.00	0.16	0.25	0.02	0.00	0.16	0.29	0.52	0.05	0.21	1.15	0.05	0.24
Al2O3	17.52	21.59	32.96	40.10	37.25	52.51	23.29	39.23	34.39	34.52	52.87	24.41	33.99	18.88	23.14	52.80
Cr2O3	0.05	0.03	0.05	0.00	0.01	0.02	0.00	0.02	0.05	0.02	0.04	0.02	0.00	0.00	0.00	0.00
FeO	22.68	28.62	3.02	22.34	1.27	12.38	24.08	23.85	3.01	1.82	11.80	18.95	2.23	17.28	20.28	13.73
MnO	0.02	0.05	0.01	0.92	0.03	0.32	0.17	0.55	0.04	0.00	0.16	0.07	0.03	0.04	0.07	0.15
MgO	8.20	8.63	1.58	2.97	0.14	1.15	14.14	2.80	0.56	0.30	1.18	16.67	0.61	12.37	18.24	1.58
CaO	0.00	0.04	0.02	0.00	0.49	0.00	0.01	0.00	0.13	0.00	0.02	0.01	0.00	0.01	0.01	0.00
Na2O	0.04	0.09	0.35	0.04	2.19	0.02	0.09	0.04	1.20	0.61	0.00	0.11	0.45	0.16	0.04	0.01
K2O	7.40	0.66	10.30	0.01	7.55	0.00	0.04	0.01	7.94	8.98	0.00	0.83	8.99	8.50	0.02	0.00
Sum	92.89	84.13	95.56	91.49	94.57	94.63	87.32	91.65	92.58	92.30	94.63	87.77	94.90	95.63	85.78	97.21
Si	2.776	5.476	3.133	2.077	3.017	8.312	5.338	2.091	3.080	3.120	8.298	5.409	3.203	2.766	5.033	8.344
Ti	0.094	0.015	0.021	0.000	0.008	0.056	0.003	0.000	0.008	0.015	0.116	0.008	0.010	0.064	0.008	0.052
Al	1.621	5.728	2.598	3.910	2.912	18.389	5.752	3.845	2.769	2.775	18.445	5.840	2.652	1.653	5.737	18.095
Cr	0.003	0.005	0.003	0.000	0.001	0.005	0.000	0.001	0.003	0.001	0.009	0.003	0.000	0.000	0.000	0.000
Fe	1.488	5.387	0.169	1.546	0.070	3.076	4.219	1.658	0.172	0.104	2.921	3.216	0.123	1.073	3.567	3.338
Mn	0.001	0.010	0.001	0.064	0.002	0.081	0.030	0.039	0.002	0.000	0.040	0.012	0.002	0.003	0.012	0.037
Mg	0.959	2.895	0.157	0.366	0.014	0.509	4.415	0.347	0.057	0.030	0.520	5.042	0.060	1.369	5.718	0.685
Ca	0.000	0.010	0.001	0.000	0.035	0.000	0.002	0.000	0.010	0.000	0.006	0.002	0.000	0.001	0.002	0.000
Na	0.006	0.039	0.045	0.006	0.282	0.012	0.037	0.006	0.159	0.081	0.000	0.043	0.058	0.023	0.016	0.006
K	0.741	0.190	0.879	0.001	0.639	0.000	0.011	0.001	0.692	0.781	0.000	0.215	0.759	0.805	0.005	0.000
Sum	7.690	19.755	7.007	7.971	6.979	30.438	19.806	7.989	6.951	6.907	30.356	19.790	6.868	7.757	20.100	30.556
XMg	0.392	0.350	0.482	0.192	0.164	0.142	0.511	0.173	0.249	0.227	0.151	0.611	0.328	0.561	0.616	0.170

Mineral name abbreviations after Kretz (1983). XMg = Mg/(Mg+Fe). All iron assumed to be ferrous.
Oxygen basis for calculating cations: Bt - 11, Chl - 28, Ms - 11, Cld - 12, St - 48, Grt - 12.

TABLE 3. REPRESENTATIVE COMPOSITIONS OF MINERALS FROM ZONES 4-6 IN RAMAH GROUP METAPELITES

Sample	F83-79	F83-79	F83-79	F83-79	F83-76	F83-76	F83-76	BR-277	BR-277	BR-169	BR-169	BR-169	BR-169	F83-131	F83-131	F83-131
Zone	4/5	4/5	4/5	4/5	5	5	5	5	5	6	6	6	6	6	6	6
Mineral	St	Ms	Bt	Chl	Bt	Ms	Chl	St	Bt	St	Bt	Grt	Ms	Grt	Bt	Ms
Code	P1	P9	P13	P30	P24	P28	P27	P1	P3	P1	P4	P5	P8	P9	P11	P22
SiO2 wt%	28.18	45.37	37.92	25.29	38.81	47.93	27.49	28.63	38.63	26.77	34.89	37.57	48.53	36.17	33.55	45.06
TiO2	0.58	0.39	1.54	0.08	0.70	0.05	0.00	0.50	1.45	0.44	1.59	0.07	0.47	0.00	1.56	0.47
Al2O3	53.31	33.24	19.25	23.36	19.14	32.59	23.02	53.46	19.48	52.42	18.54	20.48	35.97	19.99	19.10	33.00
Cr2O3	0.00	0.00	0.00	0.00	0.00	0.00	0.00	0.05	0.02	0.02	0.02	0.03	0.00	0.00	0.00	0.00
FeO	12.34	2.32	13.02	14.60	9.66	2.57	12.69	12.07	12.57	14.30	23.80	38.05	1.28	32.76	23.12	1.68
MnO	0.25	0.01	0.00	0.08	0.11	0.00	0.03	0.34	0.08	0.01	0.06	0.86	0.03	7.20	0.17	0.04
MgO	2.24	0.64	15.33	22.48	18.78	0.68	23.82	1.77	15.91	1.46	6.93	2.30	0.43	2.42	8.27	0.71
CaO	0.00	0.00	0.00	0.02	0.00	0.00	0.00	0.01	0.00	0.01	0.00	0.73	0.04	1.14	0.07	0.03
Na2O	0.01	1.10	0.24	0.05	0.28	1.30	0.02	0.00	0.19	0.01	0.13	0.05	0.59	0.07	0.05	0.55
K2O	0.00	7.61	8.68	0.01	10.05	9.81	0.10	0.01	8.98	0.01	9.74	0.03	9.17	0.00	7.99	8.85
Sum	96.91	90.68	95.98	85.97	97.53	94.93	87.17	96.84	97.31	95.45	95.70	100.17	96.51	99.75	93.88	90.39
Si	8.179	3.140	2.750	5.136	5.496	6.420	5.424	8.296	2.757	7.976	2.710	3.040	3.148	2.971	2.631	3.139
Ti	0.127	0.020	0.084	0.012	0.075	0.005	0.000	0.109	0.078	0.099	0.093	0.004	0.023	0.000	0.092	0.025
Al	18.239	2.712	1.645	5.593	3.195	5.146	5.354	18.261	1.639	18.412	1.698	1.953	2.750	1.936	1.766	2.710
Cr	0.000	0.000	0.000	0.000	0.000	0.000	0.000	0.011	0.001	0.005	0.001	0.002	0.000	0.000	0.000	0.000
Fe	2.995	0.134	0.790	2.480	1.144	0.288	2.094	2.925	0.750	3.563	1.546	2.575	0.069	2.251	1.517	0.098
Mn	0.061	0.001	0.000	0.014	0.013	0.000	0.005	0.083	0.005	0.003	0.004	0.059	0.002	0.501	0.011	0.002
Mg	0.969	0.066	1.657	6.804	3.963	0.136	7.004	0.764	1.692	0.648	0.802	0.277	0.042	0.296	0.967	0.074
Ca	0.000	0.000	0.000	0.004	0.000	0.000	0.000	0.003	0.000	0.003	0.000	0.063	0.003	0.100	0.006	0.002
Na	0.006	0.148	0.034	0.020	0.077	0.338	0.008	0.000	0.026	0.006	0.020	0.008	0.074	0.011	0.008	0.074
K	0.000	0.672	0.803	0.003	1.816	1.676	0.025	0.004	0.818	0.004	0.965	0.003	0.759	0.000	0.800	0.787
Sum	30.575	6.893	7.762	20.066	15.778	14.008	19.914	30.458	7.767	30.719	7.839	7.984	6.870	8.066	7.797	6.911
XMg	0.244	0.330	0.677	0.733	0.776	0.320	0.770	0.207	0.693	0.154	0.342	0.097	0.374	0.116	0.389	0.430

Mineral name abbreviations after Kretz (1983). XMg = Mg/(Mg+Fe). All iron assumed to be ferrous.
Oxygen basis for calculating cations: Bt - 11, Chl - 28, Ms - 11, Cld - 12, St - 48, Grt - 12.

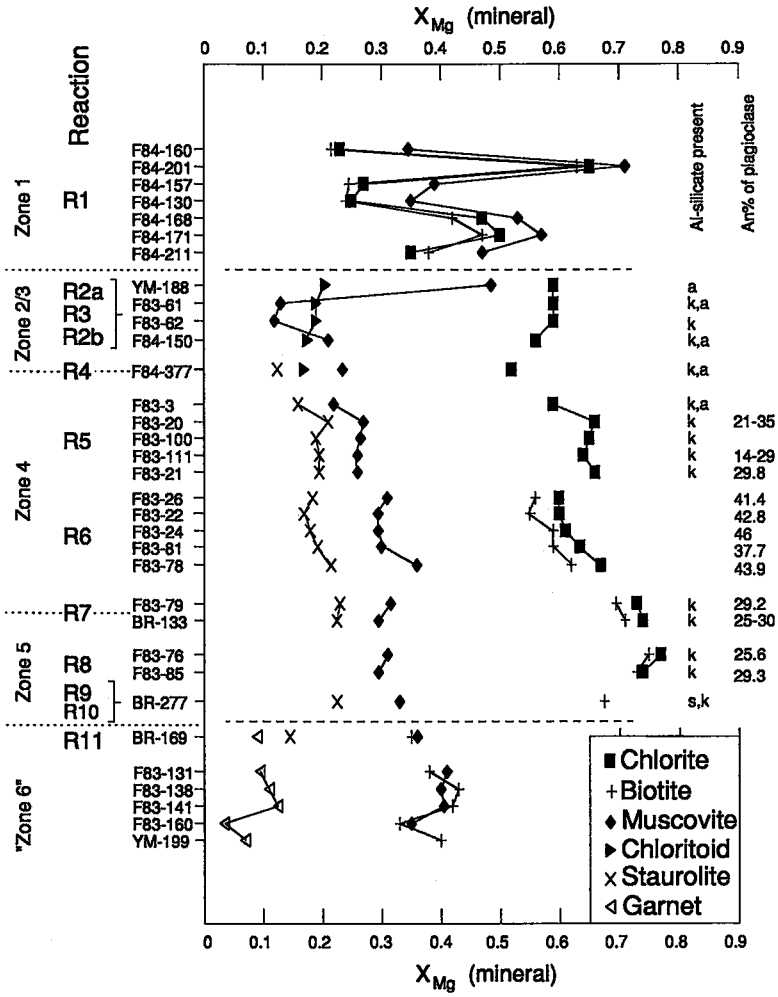

FIG. 7. Summary of compositional variations within and between the metamorphic zones. Each point represents the average result of 3–10 analyses. Abbreviations: X_{Mg} = Mg/(Mg+Fe), in which all iron is assumed to be ferrous, k: kyanite, a: andalusite, s: sillimanite.

Zone 1: Chl–Bt

This assemblage occurs exclusively in the Nullataktok Formation in the northeastern part of the Lake Kiki transect, and has been placed in the "lowest grade" zone, although it is stable over a wide range of metamorphic conditions (see below). Compositions of coexisting chlorite, biotite and muscovite from Zone 1 are shown in an AFK diagram (Fig. 8). Variation in the extent of celadonite substitution in muscovite is shown by the range in A/(A+F) (*ca.* 0.2). In contrast, the A/(A+F) ranges of coexisting biotite and chlorite are quite small (< 0.05), suggesting operation of the divariant reaction, calibrated as a geobarometer by Powell & Evans (1983) and Bucher-Nurminen (1987):

$$Ms_1 + Chl = Ms_2 + Bt + Qtz + H_2O \qquad (R1)$$

where Ms_1 is celadonite-rich, and Ms_2 is closer to "ideal" muscovite. The important exchange-vector (Thompson 1982a, b) is thus the Tschermak exchange $[(Fe,Mg)_{-1}Si_{-1}Al_2]$. Evidence of progress of R1 is indicated by many petrographic observations of biotite replacing chlorite, by the presence of crossing tie-lines in Figure 8 (Ms_2–Bt crossing Ms_1–Chl) and by the

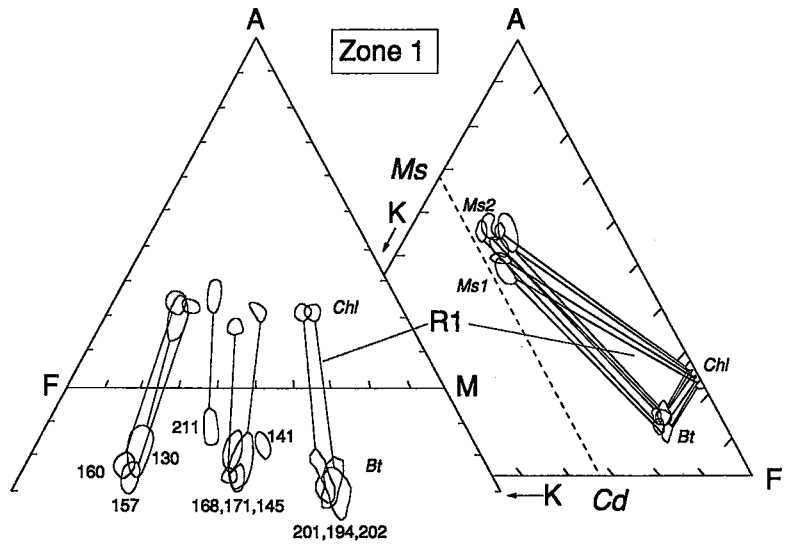

FIG. 8. (Right): Chlorite, biotite and muscovite from samples in Zone 1 plotted in the AFK diagram. The compositional variation corresponding to the Tschermak exchange $[(Fe,Mg)_{-1}Si_{-1}Al_2]$ between end members celadonite (Cd) and ideal muscovite (Ms) is indicated. Each field encloses the range of 3–10 analyses. For clarity, sample numbers are omitted. (Left): Chlorite and biotite from samples in Zone 1 plotted in the AFM diagram. All sample numbers have prefix "F84–". Each field encloses the range of results of 3–10 analyses.

decreasing modal ratio of chlorite to biotite. As the reaction proceeds, progressively Al-richer rocks become biotite-bearing, which is in accord with field observations that biotite occurs at lowest grade in Al-poor rocks (see also Wang *et al.* 1986). Significant variation in terms of Fe–Mg occurs in coexisting chlorite and biotite (Fig. 8) but, as indicated by the general parallelism of tie-lines, this variation predominantly reflects the wide range in bulk compositions.

The locations of Chl–Bt-bearing assemblages overlap spatially with those in adjacent zones owing to differences in bulk composition between the Reddick Bight – Rowsell Harbour and Nullataktok formations, and the assemblage is thus not diagnostic of Zone 1. Nonetheless, it provides a useful qualitative guide to metamorphic grade in the lower-grade rocks of the Ramah Group.

Zone 2: Cld–Chl–And and
Zone 3: Cld–Chl–Ky

These two zones are defined in Al-rich rocks, and are considered together because of the limited documentation of chlorite and chloritoid with only a single aluminosilicate in the sample suite. In contrast, several occurrences of Cld–Chl–And–Ky were found (Fig. 7), and the subassemblage Cld–Chl, which is common to both zones, is widespread.

The subassemblage Cld–Chl with or without aluminosilicate(s) occurs in the western part of the Lake Kiki section and on the northern and southern shores of Saglek Fiord, in rocks of the Reddick Bight and Rowsell Harbour formations. Biotite does not occur in these assemblages. The reason for this is clear in the AKF diagram (Fig. 9), in which it can be seen that the chloritoid-bearing assemblages are located at or above the muscovite–chlorite tie-line and hence contain one or more Al-rich phase rather than biotite.

The influence of bulk-rock X_{Mg} on the stability of chloritoid is illustrated in the AFM diagram (Fig. 9), which shows that chloritoid occurs only in rocks with intermediate to low X_{Mg} with Fe-rich chlorite and andalusite and kyanite. At higher X_{Mg}, the stable assemblage is And/Ky–Chl. The two Cld assemblages are related by the divariant reactions

$$\text{And/Ky} + \text{Chl} + \text{Qtz} = \text{Cld} + \text{H}_2\text{O} \qquad \text{(R2)}$$

which takes place as the And/Ky–Chl–Cld subtriangle sweeps to more Fe-rich compositions with increasing temperature (Thompson 1976).

Zone 2 is related to Zone 3 by the reaction isograd

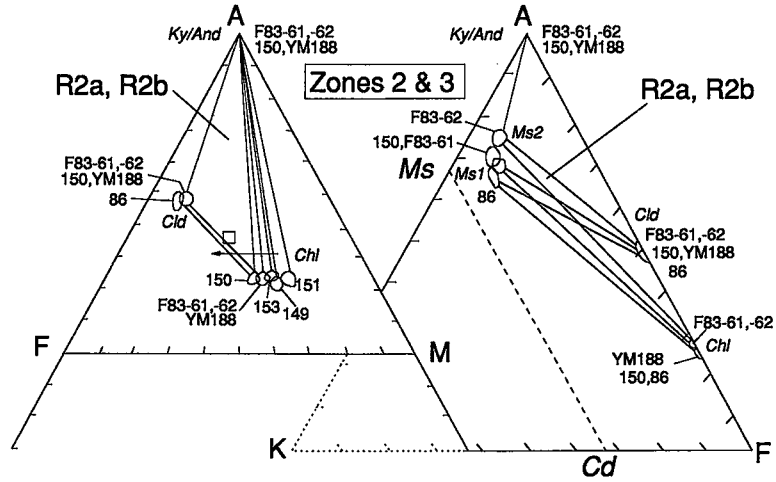

FIG. 9. (Right): Minerals from samples in Zones 2 and 3 plotted in the AKF diagram. Sample numbers without prefix are "F84–". Each field encloses the range of 3–10 analyses. The Tschermak exchange $[(Fe,Mg)_{-1}Si_{-1}Al_2]$ between end members celadonite (Cd) and ideal muscovite (Ms) is indicated. (Left): Minerals from samples in Zones 2 and 3 plotted in the AFM diagram. Each field encloses the range of 3–10 analyses. Sample numbers without prefix are "F84–". The open square represents the bulk composition of F84–150. The arrow represents the compositional change with increasing temperature, as predicted by Thompson (1976).

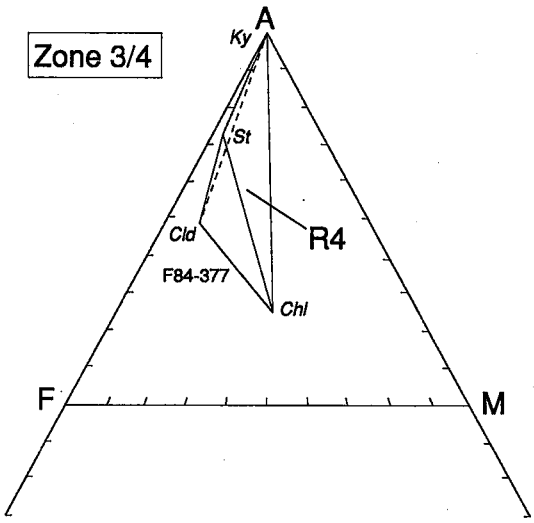

FIG. 10. Minerals from the sample containing the reaction isograd Cld + Ky = St + Chl, defining the boundary between zones 3 and 4, plotted in the AFM diagram. St–Chl is replacing Cld–Ky (stippled) as the stable mineral pair.

$$\text{And} = \text{Ky} \qquad \text{(R3)}$$

and evidence of kyanite overgrowing and replacing andalusite is seen in several samples.

Reaction isograd: Cld + Ky = St + Chl

The full reaction, which is univariant in the FMASH subsystem, is:

$$\text{Cld} + \text{Ky} = \text{St} + \text{Chl} + \text{Qtz} + \text{H}_2\text{O} \qquad \text{(R4)}$$

It marks the transition between zones 3 and 4. It was found in only one sample (F84–377, Fig. 3c) on the north shore of Saglek Fiord, *ca.* 500 m from the western boundary of the Ramah Group. In thin section, equilibrium microstructures between coexisting staurolite and chlorite are apparent, whereas chloritoid and kyanite rarely touch. Andalusite also is present, but is clearly being replaced and overgrown by kyanite, a relationship that is interpreted to represent the progress of R3.

The compositions of the coexisting phases in AFM space are shown in Figure 10, in which tie lines between both Ky–Cld and St–Chl are shown. The shape of the Ky–St–Cld subtriangle reflects the close similarity of X_{Mg} for staurolite and chloritoid, as noted by other authors (*e.g.*, Grambling 1983).

Zone 4: St–Chl

The assemblages St–Chl–Ky, St–Chl and St–Chl–Bt occur south of Saglek Fiord, predominantly in the central and eastern part of the exposed Ramah Group (Fig. 4). Figure 11 shows the locations of the assemblages in AFM space, and it is clear that they reflect variable whole-rock A/(F+M) ratios. Staurolite displays restricted compositional variation within each assemblage, whereas biotite and chlorite show larger ranges. The crossing tie-lines are due to rotation of the Ky–St–Chl subtriangle about the A apex toward Mg-richer compositions with increasing T. The spread in X_{Mg} of chlorite and biotite in the assemblages indicates that the divariant reactions

$$Ky + Chl = St + Qtz + H_2O \quad (R5)$$

$$Chl + Ms = St + Bt + Qtz + H_2O \quad (R6)$$

have taken place.

Reaction Isograd: St + Chl = Ky + Bt

This univariant assemblage, which marks the instability of the St–Chl tie-line with respect to the Ky–Bt tie-line (Fig. 12), was found in two samples (F83–79, BR–133, see Fig. 3d) from the western part of the Ramah Group, south of Saglek Fiord. The model univariant reaction is

$$St + Chl + Ms = Ky + Bt + Qtz + H_2O \quad (R7)$$

Modal proportions of minerals in the two samples indicate either a different extent of reaction progress, perhaps due to slightly different bulk-compositions; in F83–79, only a few grains of kyanite occur, whereas BR–133 is kyanite-rich, but contains only subordinate staurolite. However, in both specimens, equilibrium coexistence of kyanite and biotite is indicated by mutually stable grain-boundaries, whereas staurolite and chlorite were not observed in contact.

Zone 5: Ky–Bt

The assemblages Ky–Bt–Chl, Ky–Bt–St and Ky–Bt are stable at metamorphic grades above the breakdown of the St–Chl tie-line (Fig. 13). The three-phase assemblages record progress of the divariant reactions

$$Chl + Ms + Qtz = Ky + Bt + H_2O \quad (R8)$$

and

$$St + Ms + Qtz = Ky + Bt + H_2O \quad (R9)$$

respectively. Ky–Bt–Chl occurs in samples from the western outcrops of the Ramah Group, south of Saglek Fiord (see Fig. 3e), whereas the remaining assemblages are from Pangertok SW.

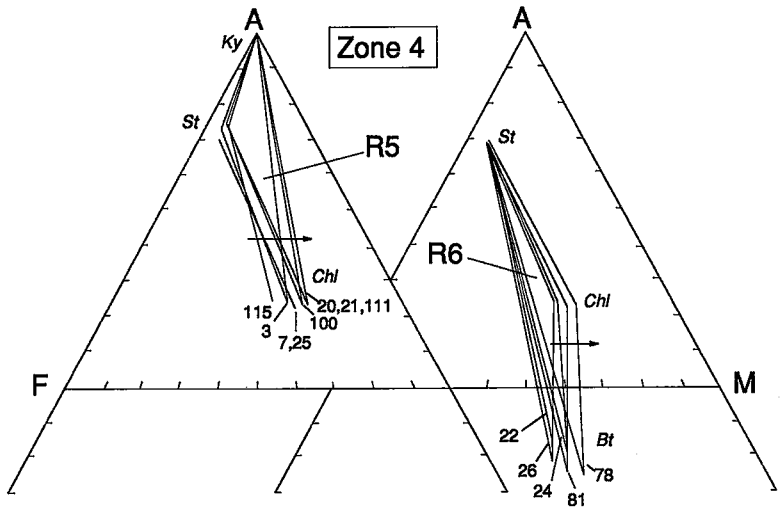

FIG. 11. Minerals from samples in Zone 4 plotted in the AFM diagram. All sample numbers have prefix "F83–". The arrows represents the compositional change with increasing temperature, as predicted by Thompson (1976).

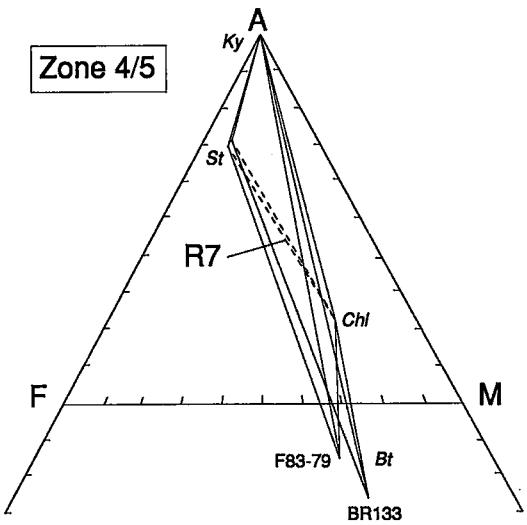

FIG. 12. Minerals from samples containing the reaction isograd St + Chl = Ky + Bt, separating Zones 4 and 5, plotted in the AFM diagram. St–Chl (dashed) has been replaced by the Ky–Bt pair.

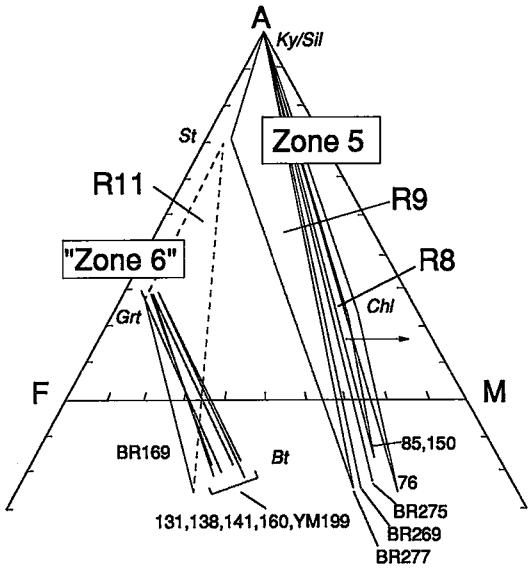

FIG. 13. Minerals from samples in Zones 5 and 6 plotted in the AFM diagram. All sample numbers without prefix are "F83–". The arrow represents the compositional change with increasing temperature, as predicted by Thompson (1976).

No assemblages recording the terminal reaction for chlorite were seen in the field. Chlorite (X_{Mg} = 0.75) occurs in the assemblage Chl–Bt at higher grade than R7 south of Saglek Fiord, whereas in Pangertok SW, prograde chlorite is absent from all pelitic assemblages. We have not found cordierite in any samples of the Ramah pelites, suggesting that chlorite was eliminated from the prograde mineralogy by the operation of reactions such as R1 or R5–8.

Three significant paragenetic changes take place between the Saglek and Pangertok SW. In Pangertok SW, (i) chlorite is absent, (ii) sillimanite (generally fibrolite), with or without kyanite, is the stable aluminosilicate, and (iii) garnet appears.

Reaction isograd: Ky = Sil

Sillimanite and kyanite are both present in BR–277, thus recording proximity to the reaction isograd

$$\text{Ky} = \text{Sil} \qquad \text{(R10)}$$

The rock is finely layered with Ky–St–Bt–Ms–Qtz- and Sil–St–Bt–Ms–Qtz-bearing pelitic layers and Sil–Bt–Qtz-bearing quartzitic layers. Sillimanite and kyanite are observed in contact, but display no apparent reaction-relationship.

"Zone" 6: Assemblages Sil–St–Bt, Grt–Bt and Grt–St–Bt

The assemblage Sil–St–Bt (Fig. 13) occurs in only one sample (BR–277, see above). The two remaining assemblages, which developed in more "F"-rich bulk compositions, are not diagnostic of particular zones, and are grouped here for convenience only.

The two-phase assemblage Grt–Bt (Fig. 3f), which is common in pelites in the Pangertok SW area, is compatible with a number of zones and thus non-diagnostic.

The stability of the assemblage Grt–St–Bt (BR–169), which is indifferent to reactions affecting the St–Chl tie-line (Fig. 13), spans a temperature range in which assemblages of zones 4 and 5 are stable.

Evidence of garnet-forming reactions is not abundant, but in BR–169, staurolite occurs as rounded relics included within garnet, and muscovite coexists with biotite throughout the thin section, consonant with operation of the divariant reaction

$$\text{St} + \text{Bt} + \text{Qtz} = \text{Grt} + \text{Ms} + \text{H}_2\text{O} \qquad \text{(R11)}$$

(Fig. 13), where staurolite was preserved because it was armored by garnet. The observation that the Grt–Bt tie-lines cut the St–Bt tie-line (Fig. 13) implies that the Grt–Bt-bearing assemblages formed at higher metamorphic grade than the St–Bt assemblages.

The assemblage Grt–Bt–Sil was not seen, such that

it is not clear if the terminal stability of staurolite in the presence of muscovite and quartz was exceeded *via* the reaction:

$$St + Ms + Qtz = Sil + Grt + Bt + H_2O \qquad (R12)$$

The garnet–biotite assemblages (Fig. 13) are not diagnostic of this reaction, as they occur in too Fe-rich a composition to be affected by it.

Construction of a Petrogenetic Grid

With the recent availability of internally consistent databases and the TWEEQU software (*e.g.*, Brown *et al.* 1988, Berman 1991), which includes solution models for several important phases, it has become feasible in some circumstances to construct petrogenetic grids using measured compositions of natural phases. Such grids should give a more precise representation of the P–T conditions undergone by the rocks under study. Unfortunately, however, the present assemblages are not ideally suited to treatment with TWEEQU, as the database lacks essential thermochemical information for magnesian staurolite and ferrous chlorite end-members, as well as appropriate solution-models for these phases, so that reactions containing intermediate compositions of these two minerals cannot be modeled. In addition, celadonite and chloritoid are not in the database, hence P–T data for Cld- and some Ms-bearing assemblages (R1, R2 and R4) cannot be obtained from TWEEQU.

However, information about the relative orientations in P–T space of some of the reactions described above can be obtained from the KFMASH petro-

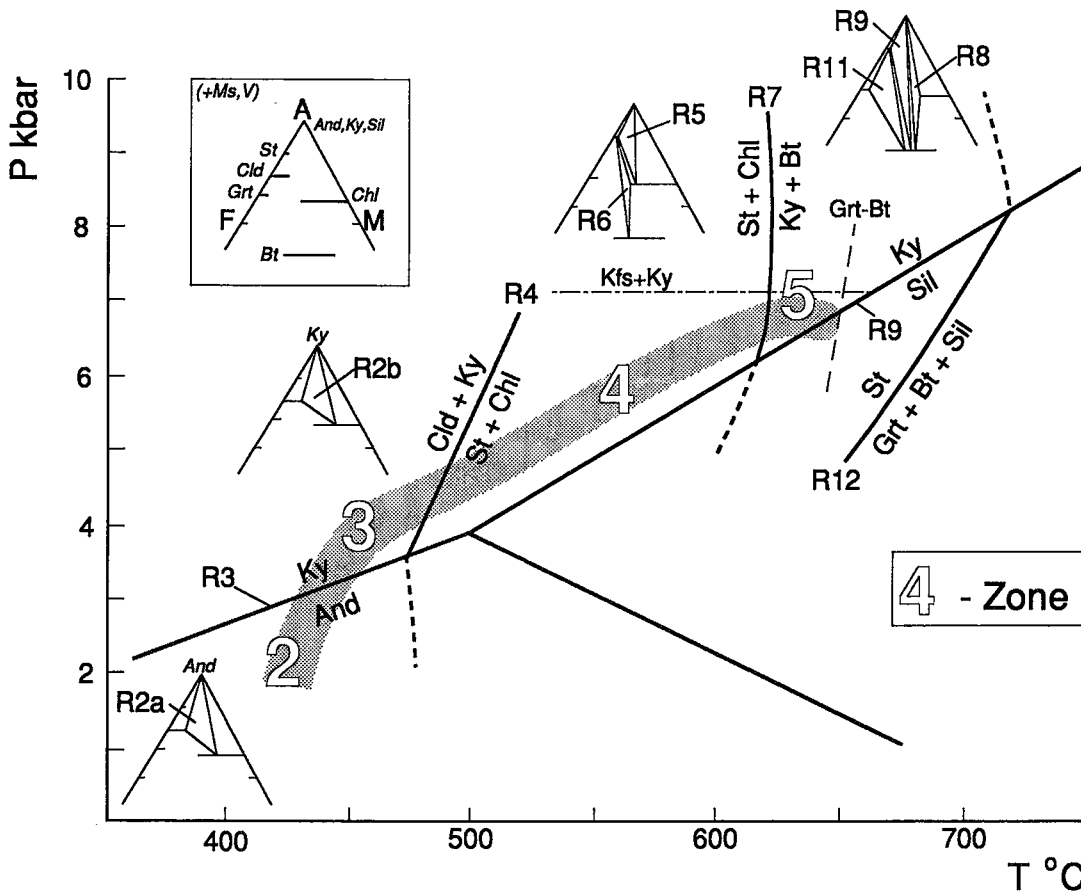

FIG. 14. P–T diagram showing the locations of reaction isograds (R3, R4, R7, R12) separating metamorphic zones 2, 3, 4 and 5 (from Spear & Cheney 1989). Inset AFM diagrams show the assemblages and reactions within each zone, as discussed in the text. The line "Kfs+Ky" is the lower limit of stably coexisting K-feldspar and kyanite (Bathograd 6 of Carmichael 1978). The line "Grt–Bt" represents the highest temperature obtained with the Grt–Bt thermometer (using TWEEQU, Berman 1991). The metamorphic field-gradient is schematically indicated by the stippled field. See text for further discussion.

genetic grid of Spear & Cheney (1989). This grid is largely based on the same database as TWEEQU, with thermodynamic data for minerals not in the database (Fe–Cld, Mg–Ctd, Mg–St, Fe–Chl) being estimated such that maximum consistency with the database was retained. Attempts to model R8 (using Mg end-members) and R9 (using Fe end-members) with TWEEQU gave results that were incompatible with the univariant reactions R4, R7 and R12 (locations taken from Spear & Cheney 1989), regardless of the activity models chosen.

Figure 14 shows the locations of zones, reactions and AFM-compatibilities with respect to univariant reactions R3, R4, R7, R9, and R12 (from Spear & Cheney 1989). The metamorphic field-gradient (MFG; Spear *et al.* 1984) crosses R3 below R4 (from Zone 2 to Zone 3), crosses R4 and R7 in the kyanite field (in Zones 3, 4 and 5), and then crosses into the sillimanite field. No evidence was found for the terminal reaction of staurolite (R12), hence the MFG crosses R9 somewhere below R12. Some P–T constraints are, however, provided by the absence of the bathograd 6 subassemblage Kfs–Ky (Carmichael 1978) and from Grt–Bt thermometry (see below), respectively.

Mineral Chemistry

In this section, the compositions and chemical variations of coexisting minerals along the metamorphic field-gradient in the Ramah Group are considered, together with patterns of zoning in individual minerals. These data provide supporting evidence of the temperature gradient within the Ramah Group, and are also necessary for the geothermobarometric calculations. Partial sets of mineral compositions are given in Tables 2 and 3, Figure 7 and in AFM and AKF diagrams above. All Fe is calculated as Fe^{2+}, an assumption that is discussed below. A full set of results of mineral analyses is available from the authors.

Muscovite

Muscovite in the Ramah Group pelites predominantly comprises the Ms (*sensu stricto*) end member, but also contains significant paragonite (Pg) and celadonite (Cd) components. X_{Pg} in muscovite generally is less than 0.2, but attains 0.4 in a few samples. There is no systematic trend of X_{Pg} with grade of metamorphism. Celadonite contents of muscovite are less than 0.1 in most samples, except in Zone 1, where they reach 0.25. X_{Mg} of muscovite is quite variable, from about 0.1 to 0.7 (Fig. 7). All AFM diagrams have been projected from ideal muscovite, but this simplification is not considered to cause a significant disturbance of the phase relations. However, inasmuch as there is a measurable and variable Cd component, muscovite should be treated as a ferromagnesian phase (as also advocated by Thompson 1982a) for the purposes of interpreting realistic reactions. No zoning was detected within individual crystals of muscovite.

Biotite

Biotite compositions are close to the annite–phlogopite series, but contain about 25% of the siderophyllite–eastonite end members. The variation in Al content of biotite is correlated with bulk composition and Al-saturation. Ti ranges between 0.06 and 0.12 atoms p.f.u. (basis: 11 atoms of oxygen). Variations in X_{Mg} are shown in Figure 7, which illustrates that biotite in Zones 1 and 6 has lower values ($X_{Mg} < 0.5$) than biotite from the other zones ($X_{Mg} > 0.5$). This variation is in accord with bulk chemical differences described above. The analyzed grains of biotite display no detectable zoning.

Chlorite

All analyzed grains of chlorite are members of the trioctahedral clinochlore–chamosite series, with low concentrations of Mn. Variability of tetrahedrally and octahedrally coordinated Al is small. There is substantial variation in X_{Mg}, however, from 0.5 to 0.8 in Zones 2–5, and from 0.2 to 0.6 in Zone 1 (Fig. 7). Individual grains are unzoned.

Chloritoid

The chloritoid is Fe-rich ($X_{Mg} \approx 0.2$; Fig. 7) and contains trace Mn. Most grains of chloritoid are too small to obtain proper analyses of core and rim, but in two samples with suitable grains (YM–188 from south of Saglek Fiord and F84–86 from just east of Lake Kiki), chloritoid is unzoned with respect to Mg and Fe, but strongly zoned with respect to Mn which, despite contents of less than 1 wt% MnO, displays a systematic rimward decrease. This pattern is consistent with growth zoning. In the absence of garnet, Mn is strongly partitioned into chloritoid, so that during prograde growth, Mn is progressively depleted from the "reservoir" (= matrix), resulting in a rimward decrease. The preservation of growth zoning suggests that retrograde effects are minor in these chloritoid-bearing assemblages.

Garnet

Garnet occurs only in the Pangertok SW area. Variations in Fe, Mg, and Mn in fourteen grains from six samples are shown in Figure 15. Grains in BR–169 and F83–138 are irregular in shape and do not display consistent patterns of zoning. Staurolite inclusions occur in one grain of garnet (BR–169), suggesting that garnet partially replaced staurolite.

Fe and Mg show no obvious correlation, but closer inspection reveals two distinct groups (I and II,

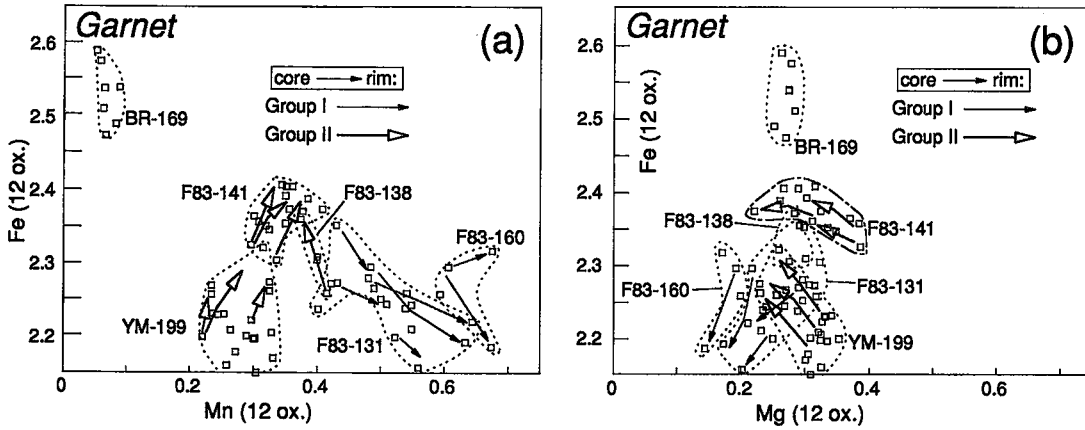

FIG. 15. Compositional variations in garnet from samples in Zone 6. Stippled fields enclose all analytical results from several grains in each sample. Arrows (Group I: filled, Group II: open) point from core toward rim analyses in zoned grains of garnet.

Fig. 15). High-Mn garnet (Group I) in general shows an increase in Mn and a decrease in Fe from core to rim, whereas both elements increase rimward in Group II. Group I is characterized by very small variations in (Fe+Mn), whereas Mn/Fe is nearly constant in Group II. Group-I garnet shows decrease in Fe and Mg from core to rim, whereas in Group II, the garnet increases in Fe and decreases in Mg toward the rim, with (Fe+Mg) remaining approximately constant.

Ca in both groups varies between 1 and 2 wt% CaO (*ca.* 3 to 7 mol% grossular), but does not show any systematic zonal variation. It is well known that in the presence of plagioclase, Al-silicate and quartz, the Ca-content of garnet is strongly pressure-dependent (*e.g.*, Kretz 1959, Ghent 1975, Martignole & Nantel 1982). However, in the garnet-bearing rocks from the Ramah Group, the lack of Al-silicates (*i.e.*, potentially variable activity of Al_2SiO_5) and the low modal amounts of plagioclase coexisting with all garnet may explain the unsystematic variation in Ca.

The zoning patterns of Fe, Mg, and Mn described above do not resemble the patterns of growth zoning widely discussed in the literature (*cf.* reviews in Tracy 1982, Cygan & Lasaga 1982, Loomis 1983), suggesting that some redistribution of elements may have occurred during or after the peak of metamorphism. The pattern in Group-I garnet (Fe and Mg decreasing and Mn increasing from core to rim) is similar to diffusion (or retrograde) zoning, particularly with respect to the Fe–Mn relationship (*e.g.*, review by Karabinos 1984). Constant (Fe+Mn) coupled with a core-to-rim increase in Mn/Fe is interpreted to result from diffusion and redistribution of elements during retrograde metamorphism (resorption), thus overprinting earlier prograde patterns. In Group-II garnet, the pattern of increasing (Fe+Mn) and decreasing Mg from core to rim may also have developed as a result of resorption during retrograde conditions.

These variations in patterns of zoning do not seem to be correlated either with mineral assemblages or geographic location. All grains of garnet coexist with biotite, muscovite, quartz, tourmaline and minor Fe–Ti oxides, and samples from both groups occur in adjacent outcrops. Although the number of samples is small (six samples with about ten well-zoned grains), the variety of patterns observed suggests that along with exchange reactions between garnet and matrix minerals, one or more diffusion-enhancing factors (*e.g.*, temperature, variable activity of H_2O and availability of fluids) were important once the peak metamorphic conditions were achieved.

Staurolite

The variations in Fe–Mg are very limited in staurolite, and core-to-rim ranges of X_{Mg} are small and unsystematic. However, the minor elements Mn and Ti generally increase toward the rim. Twenty-three grains in eleven samples were analyzed for Zn, which varies from below the detection limit to 2.21 wt% ZnO. As expected, there is a strong antithetic relationship between modal proportion of staurolite and wt% ZnO in staurolite, confirming that staurolite is the only significant Zn-bearing phase in these rocks. Zn-zoning is variable, both within and among grains; 48% of the grains show rimward increase in Zn, 17% show the opposite trend, and 35% show no measurable variation.

Feldspars

Plagioclase is the only feldspar in pelites from the areas near Saglek Fiord, whereas both K-feldspar and plagioclase occur in some samples in the Pangertok SW area. An-contents (averages or ranges) of analyzed plagioclase are shown in Figure 7. The average An-content of plagioclase in kyanite-bearing assemblages is An_{26} (n = 75 analyses, range An_{18}–An_{30}), and "normal" zoning (*i.e.*, Na-rich rim, Ca-rich core) is developed in many grains. Typical core–rim variations are from An_{25} to An_{20}. Plagioclase from kyanite-free assemblages has a higher An-content ($\sim An_{41}$, average of sixty analyses, range An_{35}–An_{46}), probably an effect of bulk composition, and displays minor normal or reverse zoning. Plagioclase and K-feldspar from the Pangertok SW area are not systematically zoned.

Patterns of zoning

Patterns of retrograde zoning in garnet from Pangertok SW (Zone 6) indicate that re-equilibration continued after the metamorphic peak in this area. In contrast, staurolite and chloritoid from Lake Kiki and Saglek Fiord areas (Zones 1–5) are unzoned or record prograde growth-related zoning, and show no evidence of post-peak re-equilibration. Normal patterns of zoning in plagioclase in kyanite-bearing, garnet-free assemblages (Zones 2–5) are interpreted to be growth-zoning phenomena due to partitioning of Na between muscovite and plagioclase. Thus, significant retrograde zoning was restricted to the higher-grade rocks (Zone 6) in the Pangertok SW area.

Fe–Mg distribution between coexisting minerals

Figure 7 shows X_{Mg} of coexisting minerals along with additional paragenetic information. In most respects, these results are in accord with the accepted pattern of X_{Mg} (*i.e.*, Grt < St < Cld < Bt < Chl < Ms). However, there are some exceptions, particularly with respect to muscovite. As noted above, all Fe has been treated as Fe^{2+}; the effect of neglecting the possible presence of Fe^{3+} is assessed below.

In Zone 1, the X_{Mg} sequence is Bt ≤ Chl < Ms (except for biotite in one sample, which has a higher X_{Mg} than coexisting chlorite: Figure 7). This relative sequence occurs despite significant absolute variations due to differences in bulk composition. However, between Zone 1 and Zones 2–5 the pattern changes. In Zones 2–5, although X_{Mg}(Bt) is still slightly smaller than X_{Mg}(Chl), both are now significantly larger than X_{Mg}(Ms). In Zones 2 and 3 (lacking biotite), X_{Mg}(Ms) varies significantly, but is invariably less than X_{Mg}(Chl), and X_{Mg}(Ms) is less than X_{Mg}(Cld) in some samples, but greater in others. In Zones 4 to 5, the relative X_{Mg} distribution is constant, with X_{Mg} in St < Cld < Ms < Bt < Chl. In garnet-bearing assemblages in "Zone 6", there is a marked decrease in X_{Mg}(Bt) such that it approximates X_{Mg}(Ms).

Thus it appears from Figure 7 that reversals of Fe–Mg distribution between muscovite and coexisting minerals (especially biotite, chlorite and possibly chloritoid) occur between Zones 1 and 2–3 and again between Zones 5 and 6 (stippled lines in Fig. 7). These are consistent both within samples and between groups of samples, and in most cases are too great in magnitude to be attributable to analytical error.

It is conceivable that the variability in X_{Mg} is due to variations in Fe^{2+}/Fe^{3+} ratio. In this context, we note that pelites in Zone 1 contain abundant graphite, whereas graphite has not been detected in Zones 2–6. In order to test the possible effect of variable Fe^{3+} on the X_{Mg} sequence, X_{Mg}(Ms) was recalculated assuming that 25, 50 and 75% of the Fe is ferric. These calculations show that for muscovite from Zones 2–5, at least 50% of the Fe would have to be Fe^{3+} to result in a "normal" sequence of X_{Mg} distribution, assuming simultaneously that none of the Fe in coexisting biotite and chlorite is Fe^{3+}. This seems unlikely, although since "partition coefficients" for Fe^{3+} between chlorite, muscovite and biotite are not known, not impossible. For muscovite in Zones 1 and 6, assumptions of variable Fe^{3+} in muscovite do not change the X_{Mg} sequence, though in this case the assumption of some Fe^{3+} in chlorite and biotite has a significant effect. However, the presence of graphite in Zone 1 would imply that Fe^{3+} contents of all phases are likely to be low. Although in the absence of direct determinations of Fe^{3+} in the coexisting minerals, these indications of reversals in X_{Mg} distribution cannot be considered to be definitive, we tentatively interpret them to be a real feature of the mineral assemblages. If so, and if muscovite is the cause, they represent an extremal state in the muscovite solid-solution, corresponding to a maximum or a minimum on binary T–X_{Mg} or P–X_{Mg} diagrams [Korzhinskii (1959) in Albee (1972)]. Such phenomena are not possible among ideal solutions, but nonideality, caused for instance by significant Fe–Mg ordering in distinct crystallographic sites, could lead to reversals (Thompson 1976). Hence our data may suggest that the Tschermak exchange involves significant cation order in Ms–Cd solid solutions. Additional analytical work, including analyses for ferric iron, is required to substantiate these suggestions.

Garnet–biotite thermometry

The Ramah Group does not contain many assemblages suitable for quantitative geothermobarometry. Coexisting garnet–biotite have been analyzed in six samples from the Pangertok SW area. Grains of garnet vary in size from <0.1 to 3 mm and in shape from subround to highly irregular, but where possible, both

TABLE 4. COMPOSITIONAL PARAMETERS AND TEMPERATURE ESTIMATES IN RAMAH GROUP PELITES FROM PANGERTOK SW

Sample	Grt#	Bt#	XAlm	XPrp	XGrs	XSps	XMg	XTi	XAl	K	T1	T2	T3
F83-131	8c	11a	0.738	0.070	0.037	0.156	0.389	0.031	0.133	0.148	525	539	550
	10r	11a	0.720	0.075	0.031	0.174	0.389	0.031	0.133	0.164	555	568	575
	18c	20a	0.714	0.081	0.035	0.170	0.411	0.036	0.197	0.164	555	569	563
	17r	20a	0.712	0.067	0.037	0.185	0.411	0.036	0.197	0.134	496	511	509
	26r	27a	0.714	0.085	0.038	0.162	0.394	0.033	0.174	0.184	595	610	605
	9c	4m	0.715	0.094	0.032	0.159	0.399	0.034	0.142	0.198	621	634	630
F83-138	5r	6a	0.760	0.091	0.028	0.121	0.448	0.022	0.132	0.147	522	533	547
	5r	7a	0.760	0.091	0.028	0.121	0.405	0.027	0.286	0.176	578	590	572
	4	18m	0.741	0.096	0.035	0.128	0.430	0.029	0.173	0.172	572	586	585
F83-141	4c	17m	0.756	0.125	0.022	0.096	0.443	0.024	0.182	0.208	640	650	640
	26c	34m	0.768	0.100	0.022	0.110	0.443	0.032	0.169	0.165	557	566	566
F83-160	1sm	6a	0.725	0.064	0.021	0.191	0.403	0.026	0.160	0.131	489	497	504
	1sm	9m	0.725	0.064	0.021	0.191	0.372	0.042	0.145	0.149	526	534	536
	1sm	11m	0.725	0.064	0.021	0.191	0.382	0.032	0.159	0.143	513	521	526
BR-169	5r	4a	0.866	0.093	0.021	0.020	0.342	0.033	0.143	0.208	640	648	653
	10r	9a	0.876	0.089	0.018	0.018	0.374	0.030	0.171	0.170	567	574	584
	14c	11a	0.857	0.097	0.025	0.022	0.385	0.033	0.204	0.180	587	597	595
YM-199	26r	24a	0.739	0.109	0.042	0.110	0.449	0.036	0.161	0.181	589	606	603
	29r	28a	0.748	0.104	0.034	0.114	0.437	0.030	0.336	0.179	584	598	570

(Grt#/Bt#) - identification numbers of analyzed grains.
Codes: r - rim, c - core, sm - small unzoned grain, a - Bt adjacent to Grt, no code - unzoned Grt, m - matrix mineral. XAlm, XPrp, XGrs and XSps are the mole fractions of almandine, pyrope, grossular and spessartine, respectively. XMg, XTi and XAl refer to Mg/Mg+Fe, Ti/Mg+Fe+^{VI}Al+Ti and ^{VI}Al/Mg+Fe+^{VI}Al+Ti, respectively.
$K = (Mg/Fe)^{Grt}/(Mg/Fe)^{Bt}$. T1 and T2 are temperatures obtained with the calibrations of Ferry & Spear (1978) and Hodges & Spear (1982), respectively. T3 is obtained with TWEEQU (Berman, 1991). All temperature estimates are in °C at ca. 6 kbar.

core and rim were analyzed. Biotite grains from two microstructural settings were analyzed, namely "rim biotite" adjacent to garnet, and "matrix biotite" away (several millimeters) from any visible grain of garnet.

It should be noted that retrograde zoning in garnet and the slow rates of diffusion for Fe–Mg in garnet compared to biotite in all likelihood cause the results obtained to be upper limits on the equilibrium temperatures at the time of cessation of Fe–Mg exchange.

Temperatures have been calculated with TWEEQU (Berman 1991) employing the activity models of Berman (1990) and McMullin *et al.* (1991) for garnet and biotite, respectively. Results and compositional parameters are given in Table 4. Temperatures from garnet core and matrix biotite are systematically higher than estimates from the rims of adjacent minerals, with differences of up to *ca.* 120°C (F83–131). This is consistent with retrograde zoning during post-peak re-equilibration. The highest temperatures obtained are 640°C and 653°C (F83–141, BR–169) which, when considered together with the coexistence of kyanite and sillimanite in some rocks from Pangertok SW, suggests maximum pressures of 6–7 kbar (Fig. 14). This is in accordance with the absence of the assemblage K-feldspar – kyanite (Bathozone 6 of Carmichael 1978). Rims of adjacent garnet and biotite grains indicate apparent temperatures down to *ca.* 500°C, suggesting significant re-equilibration during cooling following the metamorphic peak. The calculated garnet–biotite temperatures show no systematic geographic distribution within their relatively small area of occurrence south of Saglek Fiord, and are thus assumed to reflect variable degrees of post-peak re-equilibration, rather than regional differences in peak metamorphic temperatures (domainal re-equilibration, as described by Mengel & Rivers 1991).

Discussion

Although in many respects the mineral assemblages record an unexceptional metamorphic sequence along the metamorphic field-gradient, conform well to model relations in AKFM space, and yield reasonable P–T estimates, there are several points of petrological interest to which we draw attention. Bulk-composition control on the mineral assemblages is demonstrated by several related features.

(1) The persistence of stable chlorite in pelites well into middle amphibolite facies (zone 5), in close proximity to sillimanite-bearing assemblages, is unusual, and is possible only for chlorite of intermediate X_{Mg}. In this case, final breakdown of chlorite is attributed to the univariant reaction R7. No samples with coexisting

prograde chlorite and sillimanite have been observed.

(2) The absence of cordierite from all assemblages and the restriction of garnet to the highest metamorphic grade are also compatible with the intermediate range of X_{Mg} in the Ramah Group pelites. In addition, Mn contents are generally low, so that spessartine-rich garnet did not form at low metamorphic grades.

(3) In contrast to their limited range in F/M, the Ramah Group pelites display a wide range of A/(F+M), such that some lithologies are Al-saturated, whereas others are Al-undersaturated. This variation in bulk composition exerts a strong control on the presence or absence of Al-silicates (including chloritoid or staurolite) and biotite at certain grades of metamorphism, and is also responsible for changes in mineralogy between Zones 1 and 2 and between Zones 5 and 6. A critical AFM tie-line in this respect is St–Chl. Once it is breached by the Als–Bt tie-line, the occurrence of Al-silicate and biotite becomes possible over a much wider range of bulk composition.

Another point of interest is the role of the Tschermak exchange in the compositional evolution of several pairs of coexisting minerals, including those involving muscovite. This exchange vector describes the systematic decrease of the celadonite content of muscovite along the metamorphic field-gradient in the Ramah pelites. Biotite and chlorite, in contrast, do not show any similar systematic variations.

P–T Relationships and Implications for Regional Geological Evolution

Assemblages of metamorphic minerals in the Ramah Group metapelites crystallized during the later stages of D_1 or syn-D_2 (Mengel 1988, Calon & Jamison 1993) implying that these episodes of deformation occurred at the metamorphic peak. Evidence from contrasts in mineral assemblages across major faults, *e.g.*, in the Saglek Fiord area, suggests that some telescoping of the metamorphic gradient occurred after peak metamorphism. Figure 4 shows that samples from zone 3 (*e.g.*, F83–61,–62) and samples from zone 5 (*e.g.*, F83–76, –85) are separated by a few kilometers (measured perpendicular to the general NNW orientation of zone boundaries), and from Figure 14 it is apparent that these rocks from zones 3 and 5 may differ by up to 2 kbars and 150°C. This is in excess of what would be expected from a normal geothermal gradient and is in accord with shortening across the metamorphic field-gradient belt by east-directed thrusting, as suggested by Mengel (1984, 1985, 1988) and Mengel *et al.* (1991), and recently substantiated by the detailed structural work of Calon & Jamison (1993).

Metamorphic temperatures and pressures in the Ramah Group increase from north to south (to a maximum of 650°C and 6–7 kbar in Pangertok SW). This suggests burial to *ca.* 20 km depth in the externides of the Torngat Orogen, with crustal thickening occurring by tectonic assembly of thrust sheets (Mengel *et al.* 1991, Calon & Jamison 1993). A similar pattern was also described *ca.* 100 km south of the study area near Okak Bay (Van Kranendonk 1992).

The north–south variation in metamorphic grade in the Ramah Group in the study area suggests that tectonic thickening of the Ramah Group increased toward the south. However, peak temperature and pressure estimates of 700°C and 5 kbars on Ramah Group rocks from the Okak area obtained by Van Kranendonk (1992) suggest that the increase in metamorphic grade may not have extended much beyond Pangertok SW.

The tectonic evolution of the Ramah Group in the externides of the Torngat Orogen, described briefly above, contrasts strongly with that of the internides, where approximate doubling of crustal thickness during the Torngat Orogeny has been demonstrated (Mengel 1988, Mengel & Rivers 1990, 1991, Mengel *et al.* 1991, Van Kranendonk 1992).

Acknowledgements

FM acknowledges graduate and postgraduate fellowships from Århus University and Memorial University of Newfoundland and generous support from the Danish Natural Science Research Council. Field work was carried out with logistical support from the Newfoundland Department of Mines and Energy and with assistance from B. Starp and K. Staples. TR acknowledges support from NSERC. Bruce Ryan kindly supplied a few critical samples; Bruce Ryan, Martin Van Kranendonk and Dick Wardle are thanked for numerous discussions about Ramah Group geology over the years, and Rob Berman is thanked for help with TWEEQU. Dugald Carmichael, Peter Thompson, Robert F. Martin and Marc St-Onge are thanked for information and for critical, but very thorough and constructive comments, which improved the paper significantly. This is LITHOPROBE contribution number 551.

References

Albee, A.L. (1972): Metamorphism of pelitic schists: reaction relations of chloritoid and staurolite. *Geol. Soc. Am. Bull.* **83**, 3249-3268.

Bence, A.E. & Albee, A.L. (1968): Empirical correction factors for the electron microanalysis of silicates and oxides. *J. Geol.* **76**, 382-403.

Berman, R.G. (1990): Mixing properties of Ca–Mg–Fe–Mn garnets. *Am. Mineral.* **75**, 328-344.

_____ (1991): Thermobarometry using multi-equilibrium calculations: a new technique, with petrological applications. *Can. Mineral.* **29**, 833-855.

BROWN, T.H., BERMAN, R.G. & PERKINS, E.H. (1988): GEØ-CALC: software package for calculation and display of pressure – temperature – composition phase diagrams using an IBM or compatible personal computer. *Comput. & Geosci.* **14**, 279-289.

BUCHER-NURMINEN, K. (1987): A recalibration of the chlorite – biotite – muscovite geobarometer. *Contrib. Mineral. Petrol.* **96**, 519-522.

CALON, T. & JAMISON, J. (1993): Structural evolution of the Eastern Borderland of the Torngat Orogen, Kiki Lake transect, Saglek Fiord area, northern Labrador. *In* Eastern Canadian Shield Onshore–Offshore Transect (R. J. Wardle & J. Hall, eds.). *LITHOPROBE Rep.* **32**, 90-112.

CARMICHAEL, D.M. (1978): Metamorphic bathozones and bathograds: a measure of the depth of post-metamorphic uplift and erosion on the regional scale. *Am. J. Sci.* **278**, 769-797.

CHINNER, G.A. (1960): Pelitic gneisses with varying ferrous/ferric ratios from Glen Clova, Angus, Scotland. *J. Petrol.* **1**, 178-217.

CYGAN, R.T. & LASAGA, A.C. (1982): Crystal growth and the formation of chemical zoning in garnets. *Contrib. Mineral. Petrol.* **79**, 187-200.

ERMANOVICS, I.F. & VAN KRANENDONK, M. (1990): The Torngat Orogen in the North River – Nutak transect area of Nain and Churchill provinces. *Geosci. Canada* **17**, 279-283.

———, ———, CORRIVEAU, L., MENGEL, F., BRIDGWATER, D. & SHERLOCK, R. (1989): The boundary zone of the Nain – Churchill provinces in the North River – Nutak map areas, Labrador. *Geol. Surv. Can., Pap.* **89-1C**, 385-394.

FERRY, J.M. & SPEAR, F.S. (1978): Experimental calibration of the partitioning of Fe and Mg between biotite and garnet. *Contrib. Mineral. Petrol.* **66**, 113-117.

GHENT, E.D. (1975): Temperature, pressure, and mixed-volatile equilibria attending metamorphism of staurolite–kyanite-bearing assemblages, Esplanade Range, British Columbia. *Geol. Soc. Am. Bull.* **86**, 1654-1660.

GRAMBLING, J.A. (1983): Reversals in Fe–Mg partitioning between chloritoid and staurolite. *Am. Mineral.* **68**, 373-388.

HODGES, K.V. & SPEAR, F.S. (1982): Geothermometry, geobarometry and the Al_2SiO_5 triple point at Mt. Moosilauke, New Hampshire. *Am. Mineral.* **67**, 1118-1134.

HOFFMAN, P.F. (1988): United plates of America, the birth of a craton: Early Proterozoic assembly and growth of Laurentia. *Ann. Rev. Earth Planet. Sci.* **16**, 543-603.

KARABINOS, P. (1984): Polymetamorphic garnet zoning from southeastern Vermont. *Am. J. Sci.* **284**, 1008-1025.

KEITH, L.H., CRUMMETT, W., DEEGAN, J., JR., LIBBY, R.A., TAYLOR, J.K. & WENTLER, G. (1983): Principles of environmental analysis. *Anal. Chem.* **55**, 2210-2218.

KNIGHT, I. (1973): The Ramah Group between Nachvak Fjord and Bears Gut, Labrador. *Geol. Surv. Can., Pap.* **73-1A**, 156-161.

——— & MORGAN, W.C. (1977): Stratigraphic subdivision of the Aphebian Ramah Group, northern Labrador. *Geol. Surv. Can., Pap.* **77-15**.

——— & ——— (1981): The Aphebian Ramah Group, northern Labrador. *In* Proterozoic Basins of Canada (F.H.A. Campbell, ed.). *Geol. Surv. Can., Pap.* **81-10**, 313-330.

KORZHINSKII, D.S. (1959): *Physicochemical Basis of the Analysis of the Paragenesis of Minerals.* Consultants Bureau, New York.

KRETZ, R. (1959): Chemical study of garnet, biotite, and hornblende from gneisses of southwestern Quebec, with emphasis on distribution of elements in coexisting minerals. *J. Geol.* **67**, 371-402.

——— (1983): Symbols for rock-forming minerals. *Am. Mineral.* **68**, 277-279.

LOOMIS, T. P. (1983): Compositional zoning of crystals: a record of growth and reaction history. *In* Kinetics and Equilibrium in Mineral Reactions (S.K. Saxena, ed.). Springer-Verlag, New York, N.Y. (1-60).

MARTIGNOLE, J. & NANTEL, S. (1982): Geothermobarometry of cordierite-bearing metapelites near the Morin anorthosite complex, Grenville Province, Québec. *Can. Mineral.* **20**, 307-318.

MCMULLIN, D.W.A., BERMAN, R.G. & GREENWOOD, H.J. (1991): Calibration of the SGAM thermobarometer for pelitic rocks using data from phase-equilibrium experiments and natural assemblages. *Can. Mineral.* **29**, 889-908.

MENGEL, F. (1984): Preliminary results of mapping in the Ramah Group and adjacent gneisses south of Saglek Fiord, northern Labrador. *In* Current Research. *Nfld. Dep. Mines and Energy, Mineral. Dev. Div., Rep.* **84-1**, 21-29.

——— (1985): Nain–Churchill province boundary: a preliminary report on a cross-section through the Hudsonian front in the Saglek Fiord area, northern Labrador. *In* Current Research. *Nfld. Dep. Mines and Energy, Mineral. Dev. Div., Rep.* **85-1**, 33-42.

——— (1988): *Thermotectonic Evolution of the Proterozoic – Archean Boundary in the Saglek Area, Northern Labrador.* Ph.D. thesis, Memorial University of Newfoundland, St. John's, Newfoundland.

——— & RIVERS, T. (1990): The synmetamorphic P–T–t path of granulite facies gneisses from Torngat orogen, and its bearing on their tectonic history. *Geosci. Canada* **17**, 288-293.

_____ & _____ (1991): Decompression reactions and P–T conditions in high-grade rocks, northern Labrador: P–T–t paths from individual samples and implications for early Proterozoic tectonic evolution. *J. Petrol.* **32**, 139-167.

_____, _____ & REYNOLDS, P. (1991): Lithotectonic elements and tectonic evolution of Torngat Orogen, Saglek Fiord, northern Labrador. *Can. J. Earth Sci.* **28**, 1407-1423.

MORGAN, W.C. (1975): Geology of the Precambrian Ramah Group and basement rocks in the Nachvak fiord – Saglek fiord area, north Labrador. *Geol. Surv. Can., Pap.* **74-54**.

POWELL, R. (1978): *Equilibrium Thermodynamics in Petrology.* Harper & Row, London, U.K.

_____ & EVANS, J.A. (1983): A new geobarometer for the assemblage biotite – muscovite – chlorite – quartz. *J. metamorphic Geol.* **1**, 331-336.

SPEAR, F.S. & CHENEY, J.T. (1989): A petrogenetic grid for pelitic schists in the system SiO_2–Al_2O_3–FeO–MgO–K_2O–H_2O. *Contrib. Mineral. Petrol.* **101**, 149-164.

_____, SELVERSTONE, J., HICKMOTT, D., CROWLEY, P. & HODGES, K.V. (1984): P–T paths from garnet zoning: a new technique for deciphering tectonic processes in crystalline terranes. *Geology* **12**, 87-90.

THOMPSON, A.B. (1976): Mineral reactions in pelitic rocks. I. Prediction of P–T–X(Fe–Mg) phase relations. *Am. J. Sci.* **276**, 401-424.

THOMPSON, J.B., JR. (1957): The graphical analysis of mineral assemblages in pelitic schists. *Am. Mineral.* **42**, 842-858.

_____ (1982a): Composition space: an algebraic and geometric approach. *In* Characterization of Metamorphism through Mineral Equilibria (J.M. Ferry, ed.). *Rev. Mineral.* **10**, 1-31.

_____ (1982b): Reaction space: an algebraic and geometric approach. *In* Characterization of Metamorphism through Mineral Equilibria (J.M. Ferry, ed.). *Rev. Mineral.* **10**, 33-52.

TRACY, R.J. (1982): Compositional zoning and inclusions in metamorphic minerals. *In* Characterization of Metamorphism through Mineral Equilibria (J.M. Ferry, ed.). *Rev. Mineral.* **10**, 355-397.

VAN KRANENDONK, M.J. (1990): Structural history and geotectonic evolution of the eastern Torngat Orogen in the North River map area, Labrador. *Geol. Surv. Can., Pap.* **90-1C**, 81-96.

_____ (1992): *Geological Evolution of the Archean Nain Province and the Early Proterozoic Torngat Orogen as Seen Along a Transect in the North River – Nutak Map Area, Northern Labrador, Canada.* Ph.D. thesis, Queen's Univ., Kingston, Ontario.

_____ & ERMANOVICS, I.F. (1990): Structural evolution of the Hudsonian Torngat Orogen in the North River map area, Labrador: evidence for east–west transpressive collision of Nain and Rae continental blocks. *Geosci. Canada* **17**, 283-288.

WANG, G., BANNO, S. & TAKEUCHI, K. (1986): Reactions to define the biotite isograd in the Ryoke metamorphic belt, Kii Peninsula, Japan. *Contrib. Mineral. Petrol.* **93**, 9-17.

WARDLE, R.J. (1983): Nain–Churchill Province cross-section, Nachvak Fiord, northern Labrador. *In* Current Research. *Nfld. Dep. Mines and Energy, Mineral. Dev. Div., Rep.* **83-1**, 78-90.

Received January 25, 1993, revised manuscript accepted March 22, 1994.

APPENDIX: ANALYTICAL TECHNIQUES

Major-element analyses of Ramah Group pelites were carried out by atomic absorption spectrometry using a Perkin–Elmer spectrometer housed at the Department of Earth Sciences, Memorial University on Newfoundland, and operated by G. Andrews. Prior to analysis, 0.1000 g of sample was dissolved in a solution of 5 mL HF, 50 mL saturated H_3BO_3, and 145 mL H_2O, and heated on a steam bath for *ca.* 12 hrs. FeO was determined by titration in ferrous ammonium sulfate, and Fe_2O_3 was considered equal to $Fe_2^{3+}O_3^{tot}$ – 1.1 FeO. P_2O_5 was determined by colorimetry, and loss on ignition (LOI) was determined after heating approximately 1.5 g of sample at *ca.* 1000°C for 2–3 hrs.

Minerals were analyzed with a JEOL JXA–50A electron microprobe in the Department of Earth Sciences, Memorial University of Newfoundland. This instrument was fully automated and equipped with three wavelength-dispersion spectrometers and a Krisel control unit operating through a PDP–11 computer. Counts were collected for 30 seconds or until 60,000 counts were recorded. The beam current was 22 nA, and the accelerating voltage, 15 kV. For all minerals, a beam diameter of 1–2 μm was used. "Alpha"-corrections (Bence & Albee 1968) were used in data reduction, and a variety of calibrations, based on standards appropriate for the mineral being analyzed, were employed. For most elements, the typical lower limit of detection (LLD) is about 0.03 wt% oxide, giving average levels of quantification (*ca.* 3 × LLD, Keith *et al.* 1983) of *ca.* 0.1 wt% oxide (Mengel 1988).